# Gene expression profiling and the isocitrate dehydrogenase mutational landscape of temozolomide-resistant glioblastoma

WU-FU CHEN[1,2*], JIMMY MING-JUNG CHUANG[1*], SAN-NAN YANG[3,4], NAN-FU CHEN[5,6], MANOJIT BHATTACHARYA[7], HSIN-TZU LIU[8], KULDEEP DHAMA[9], CHIRANJIB CHAKRABORTY[10] and ZHI-HONG WEN[2]

[1]Department of Neurosurgery, Kaohsiung Chang Gung Memorial Hospital and Chang Gung University College of Medicine, Kaohsiung 83301, Taiwan, R.O.C.; [2]Department of Marine Biotechnology and Resources, National Sun Yat-sen University, Kaohsiung 80424, Taiwan, R.O.C.; [3]Department of Pediatrics, E-DA Hospital, School of Medicine, College of Medicine I-Shou University, Kaohsiung 82445, Taiwan, R.O.C.; [4]School of Medicine for International Students, College of Medicine, I-Shou University, Kaohsiung 82445, Taiwan, R.O.C.; [5]Division of Neurosurgery, Department of Surgery, Kaohsiung Armed Forces General Hospital, Kaohsiung 80284, Taiwan, R.O.C.; [6]Center for General Education, Cheng Shiu University, Kaohsiung 833301, Taiwan, R.O.C.; [7]Department of Zoology, Fakir Mohan University, Balasore, Odisha 756089, India; [8]Department of Medical Research, Hualien Tzu Chi Hospital, Buddhist Tzu Chi Medical Foundation, Hualien 970374, Taiwan, R.O.C.; [9]Division of Pathology, Indian Council of Agriculture Research-Indian Veterinary Research Institute, Izatnagar, Bareilly, Uttar Pradesh 243122, India; [10]Department of Biotechnology, School of Life Science and Biotechnology, Adamas University, Kolkata, West Bengal 700126, India

Received September 21, 2023; Accepted April 9, 2024

DOI: 10.3892/ol.2024.14511

**Abstract.** Glioblastoma multiforme (GBM) is an aggressive brain cancer that occurs more frequently than other brain tumors. The present study aimed to reveal a novel mechanism of temozolomide resistance in GBM using bioinformatics and wet lab analyses, including meta-Z analysis, Kaplan-Meier survival analysis, protein-protein interaction (PPI) network establishment, cluster analysis of co-expressed gene networks, and hierarchical clustering of upregulated and downregulated genes. Next-generation sequencing and quantitative PCR analyses revealed downregulated [tyrosine kinase with immunoglobulin and epidermal growth factor homology domains 1 (*TIE1*), calcium voltage-gated channel auxiliary subunit α2Δ1 (*CACNA2D1*), calpain 6 (*CAPN6*) and a disintegrin and metalloproteinase with thrombospondin motifs 6 (*ADAMTS6*)] and upregulated [serum amyloid (*SA*)*A1*, *SAA2*, growth differentiation factor 15 (*GDF15*) and ubiquitin specific peptidase 26 (*USP26*)] genes. Different statistical models were developed for these genes using the Z-score for P-value conversion, and Kaplan-Meier plots were constructed using several patient cohorts with brain tumors. The highest number of nodes was observed in the PPI network was for *ADAMTS6* and *TIE1*. The PPI network model for all genes contained 35 nodes and 241 edges. Immunohistochemical staining was performed using isocitrate dehydrogenase (IDH)-wild-type or IDH-mutant GBM samples from patients and a significant upregulation of TIE1 ($P<0.001$) and CAPN6 ($P<0.05$) protein expression was demonstrated in IDH-mutant GBM in comparison with IDH-wild-type GBM. Structural analysis revealed an IDH-mutant model demonstrating the mutant residues (R132, R140 and R172). The findings of the present study will help the future development of novel biomarkers and therapeutics for brain tumors.

*Correspondence to:* Professor Chiranjib Chakraborty, Department of Biotechnology, School of Life Science and Biotechnology, Adamas University, Barasat Barrackpore Road, Kolkata, West Bengal 700126, India
E-mail: drchiranjib@yahoo.com

Professor Zhi-Hong Wen, Department of Marine Biotechnology and Resources, National Sun Yat-sen University, 70 Lien-Hai Road, Kaohsiung 80424, Taiwan, R.O.C.
E-mail: wzh@mail.nsysu.edu.tw

*Contributed equally

*Key words:* glioblastoma multiforme, temozolomide resistance, isocitrate dehydrogenase mutation, gene expression

## Introduction

Malignant and non-malignant tumors of the central nervous system, including the brain, are a burden to society. They are diagnosed at a rate of 0.55 per 0.1 million individuals in a range of countries (1); however, malignancy is unusual in the USA and accounts for an unequal burden of cancer mortality owing to its augmented fatality rate (2). An average annual mortality rate of 4.43 per 100,000 individuals was recorded in those with malignant CNS tumors (3). Among these tumors, several types are gliomas, which are classified as malignant transformations of glial cells. Researchers have noted the occurrence of malignant gliomas in ~5 cases per 1 million people (4). It has also been observed that the considerable

mortality and morbidity rates associated with malignant gliomas are due to inadequate treatment efficacy and the use of aggressive therapies in the USA (5). During the calculation of glioma mortality from 1995 to 2018, it was noted that the rate declined by 0.4% per year, but an increased mortality rate was observed in older adults >80 years of age (6). On the other hand, Upadhyaya *et al* (7) found that high-grade glioma contributed to 66% of the mortality in the children population.

Glioblastoma multiforme (GBM) is a type of glioma and central nervous system tumor that can originate from ≥3 possible precursor cells: Neural stem cells (NSC), NSC-derived astrocytes and oligodendrocyte precursor cells (8). Based on their growth, gliomas were categorized into four groups (grades 1-4). Grade 4 astrocytomas are also known as GBMs. According to the World Health Organization (WHO), GBM constitutes ~16% of all brain tumors and 54% of all gliomas (9). Stupp *et al* (10) developed a standard protocol, the addition of temozolomide (TMZ) to radiotherapy (RT), for treating GBMs, which is followed by many clinicians. The tumors are surgically resected according to this protocol. Subsequently, postoperative ionizing radiation is applied alongside adjuvant temozolomide chemotherapy (10). Ionizing radiation and chemotherapy act through common pathways that induce DNA damage and cell death. They can act directly or indirectly by generating reactive oxygen species (11).

However, multidrug resistance (MDR) limits advancements in the treatment of brain tumors. MDR is a significant global problem associated with a series of processes that primarily account for chemotherapeutic drug resistance (12). Glutathione S-transferase is a group of multifunctional proteins involved in MDR. These enzymes belong to a superfamily of detoxification enzymes (13). Therefore, it is necessary to study MDR patterns in brain cancers such as GBMs, gliomas, medulloblastomas and neuroblastomas. GBMs are highly resistant to most treatments owing to their cellular heterogeneity (14). Intense clonal plasticity has also been reported. Moreover, cancer stem cells may inhibit TMZ- and RT-induced cell death (15). Thus, it is necessary to further understand GBM-associated genes and their role in chemotherapy resistance.

Several studies have reported that gene expression is responsible for MDR and chemoresistance in brain tumors (16-18). Studies have investigated alterations in the gene expression profiles of several types of brain tumors under different therapeutic conditions. Ngo and Harley assessed the global gene expression profile alterations in GBMs during therapy with the antineoplastic drug TMZ. Yao *et al* (19) illustrated the gene expression profiles of GBM resistance and identified two candidate genes, Fanconi anemia complementation group D2 and squalene epoxidase, linked to ferroptosis-related chemoresistance in GBMs. Nevertheless, there is a knowledge gap in the gene expression profiling of TMZ-resistant GBM and it is necessary to understand the gene expression profiles of drug-resistant GBM cell lines. Therefore, the present study aimed to assess the downregulated and upregulated genes in TMZ-resistant GBM. Previous studies have discussed the role of different mutations in TMZ-resistant GBM, such as anaplastic lymphoma kinase mutations (20). In contrast, O6-methylguanine-DNA methyltransferase overexpression is widely used as a biomarker to predict which patients with GBM will be unsuitable for TMZ treatment (21).

The WHO has classified GBM into two types: Isocitrate dehydrogenase (IDH)-wild-type and IDH-mutant, which possess different genetic, epigenetic and transcriptional characteristics (22). Several studies have reported that patients with IDH-mutant GBMs have improved outcomes after TMZ treatment (23). Therefore, an enhanced understanding of the IDH mutational landscape in TMZ-resistant GBM cells is required. Therefore, the present study aimed to assess the IDH mutational landscape in TMZ-resistant GBMs.

Mutations in IDH are significant factors associated with several human malignancies. Three IDH isoforms are present in humans: IDH1 is found in peroxisomes and the cytoplasm, whereas IDH2 and IDH3 are found in the mitochondrial matrix (20,24). Han *et al* (24) described the potential molecular mechanisms underlying IDH mutations in gliomas. Wild-type IDH enzymes (IDH1 and IDH2) transform isocitrate into α-ketoglutarate (α-KG), reducing $NAD(P)^+$ to NAD(P)H in the Krebs cycle. The IDH heterodimer is found in cells; thus, wild-type IDH serves a significant role in the Krebs cycle and exhibits regular activity. However, a mutation in one part of the IDH heterodimer produces D-(R)-2-hydroxyglutarate (D-2HG) from α-KG. Simultaneously, the R132H mutation in each part of the IDH homodimer (two homodimers of IDH from the IDH heterodimer) results in an inactive IDH. Moreover, IDH1 mutants result from epigenome modifications. Epigenetic reprogramming has been reported to be involved in histone modifications, DNA methylation and aberrant chromatin states in several cancers, including gliomas. Molecular targeting approaches, such as targeting redox homeostasis, have also been used to improve the efficiency of therapeutics against IDH-mutated gliomas (24). Additionally, immunotherapies have been used as advanced therapeutics against IDH-mutated gliomas (24). IDH1 mutations are also frequently found in secondary GBMs and are responsible for 73% of secondary GBMs. However, they are not common in primary GBMs and are responsible for only 3.7% of clinical cases (25). Several studies have reported that patients with IDH-mutant GBMs have improved outcomes with TMZ treatment (23,26). Qi *et al* (27) reported that patients with IDH-mutant secondary GBMs had improved TMZ treatment outcomes and prolonged survival. Therefore, it is necessary to understand the gene expression in TMZ-resistant GBM cells, the structure of IDH, and its mutational landscape in GBMs.

The present study aimed to assess the gene expression profiles of TMZ-resistant GBM and the IDH mutational landscapes in GBM in two ways: First, the expression of the genes associated with TMZ resistance was determined. GBM GBM8401-resistant cells were analyzed using next-generation sequencing (NGS) and RNA sequencing (RNA-seq) to assess the expression profiles of downregulated and upregulated genes. Meta-Z analysis was also performed using the Prediction of Clinical Outcomes from Genomic Profiles (PRECOG) system to identify all the upregulated and downregulated genes in TMZ-resistant GBM. Kaplan-Meier (KM) survival analysis, *in silico* gene expression pattern analysis, protein-protein interaction (PPI) network establishment, cluster analysis of co-expressed gene networks, and hierarchical clustering of all upregulated and downregulated genes were performed. Second, an immune-histochemical staining assay was performed to evaluate the upregulated

and downregulated genes in the wild-type and mutant IDH cells. The relative gene expression intensity in these cells was also evaluated. Finally, the mutational landscape of IDH in GBMs was demonstrated using *in silico* modeling. Meta-Z and KM survival analyses were performed in different brain cancers, such as astrocytomas, gliomas, medulloblastomas, meningiomas and neuroblastomas, along with GBMs, for all upregulated and downregulated genes. The present study also aimed to determine the prognostic and therapeutic landscape of genes in all human brain cancers, including GBM.

## Materials and methods

*Cell culture and generation of chemotherapy drug-resistant GBM cell lines*. The human brain malignant glioma GBM8401 cell line was purchased from the Bioresource Collection and Research Center (Hsinchu, Taiwan). TMZ-resistant cells were induced in the GBM8401 cell line using 200 $\mu$M TMZ-containing medium, with the medium changed every 2-3 days for 140 days (28). TMZ was purchased from Sigma-Aldrich (Merck KGaA). GBM8401 and TMZ-resistant GBM8401 cells were maintained in RPMI1640 medium (Gibco; Thermo Fisher Scientific, Inc.) supplemented with 10% heat-inactivated fetal bovine serum (Gibco; Thermo Fisher Scientific, Inc.), 50 U/ml penicillin and 50 mg/ml streptomycin (Sigma-Aldrich; Merck KGaA). Cell lines were maintained in a humidified atmosphere of 5% $CO_2$ mixed with 95% air at 37˚C. These cells were used for subsequent experiments.

*Cell viability assay*. Anti-TMZ GBM cell line viability was determined using MTT assays. Cells were seeded in 96-well plates and 20 $\mu$l of 5 mg/ml MTT (Sigma-Aldrich; Merck KGaA) was added at the end of the exposure time. The cells were incubated at 37˚C for 4 h and then medium was carefully removed. Dimethyl sulfoxide (100 $\mu$l) was added to each well and the absorbance was measured at 570 nm using a microplate spectrophotometer (BioTek Epoch; Agilent Technologies, Inc.).

*RNA-seq using NGS*. The RNA expression profiles of TMZ-resistant GBM8401 cells were analyzed using NGS. NGS transcriptome sequencing and data analyses were performed by Welgene Biotech Co., Ltd. (Taipei, Taiwan). Total RNA was extracted using TRIzol™ Reagent (Invitrogen™; Thermo Fisher Scientific, Inc.) according to the manufacturer's instructions. The SureSelect Strand-Specific RNA Library Preparation Kit (cat. no. G9691B; Agilent Technologies, Inc.) was used for library construction, followed by AMPure XP beads (cat. no. A63882; Beckman Coulter, Inc.). The loading concentration was 250 pM. Paired-end sequencing with a read length of 150 bp was performed using a NovaSeq 6000 S4 reagent kit (cat. no. 20012866; Illumina, Inc.) on an Illumina NovaSeq 6000 System (Illumina, Inc.). RNA library quantification was performed using the Agilent 4150 TapeStation System (cat. no. G2992AA; Agilent Technologies Deutschland GmbH) and High Sensitivity D1000 ScreenTape Assay (cat. no. 5067-5585; Agilent Technologies Deutschland GmbH). Sequencing data (FASTQ reads) were generated using the pipeline of Welgene Biotech Co., Ltd. based on the base-calling program bcl2fastq v2.20 of Illumina, Inc. Base calls were converted using the official Illumina, Inc. tool, bcl2fastq2 conversion software version 2.19, which was used to convert the BCL files from the Illumina sequencing systems. Both adaptor clipping and sequence quality trimming of the Illumina FASTQ data were performed using Trimmomatic version 0.36 (29). HISAT2 uses the global GFM index (graph FM index) and a large set of small GFM indices that collectively cover the entire genome for rapid and accurate alignment (30). Differential expression analysis was performed using Cuffdiff (@cufflinks 2.2.1) with genome bias detection/correction and in-house Welgene programs (31). The RNA-seq data in the present publication have been deposited in the NCBI Gene Expression Omnibus and are accessible through the GEO Series accession number GSE234762 (https://www.ncbi.nlm.nih.gov/geo).

*Relative quantification of RNA expression*. Total cellular RNA was isolated using TRIzol Reagent (Invitrogen; Thermo Fisher Scientific, Inc.). Equal amounts of total RNA were reverse transcribed into cDNA using the iScriptTMcDNA Synthesis Kit (cat. no. 1708891; Bio-Rad Laboratories, Inc.). The following conditions were used for PCR: 25˚C for 5 min (primer annealing), 46˚C for 20 min (reverse transcription), 95˚C for 1 min (inactivation) and 4˚C holds. Reverse transcripts were amplified and quantified using the CFX96TM Real-time PCR Detection System (Bio-Rad Laboratories, Inc.). The iQTM SYBR Green Supermix (Bio-Rad Laboratories, Inc.) was monitored using a CFX96TM Real-time System equipped with CFX ManagerTM software (version 3.1; Bio-Rad Laboratories, Inc.). The PCR program was as follows: 95˚C for 3 min; 40 cycles of 95˚C for 30 sec, 56˚C for 30 sec; and 72˚C for 50 sec. The expression levels of target genes were quantified relative to the expression level of GAPDH as an internal control for normalization using the $2^{-\Delta\Delta Cq}$ method (32). Primer sequences are listed in Table I.

*PRECOG analysis to comprehend the meta-Z analysis of all upregulated and downregulated genes from TMZ-resistant GBM8401 cells*. PRECOG analysis (https://precog.stanford.edu/) was performed for all upregulated and downregulated genes identified using meta-Z analysis across the brain tumor subtypes. The server helped to predict clinical outcomes from genomic profiles and determine the prognostic landscape of genes in all human cancers (33). Different brain cancers, including astrocytomas, GBMs, gliomas, medulloblastomas, meningiomas and neuroblastomas, were considered in this analysis. In the present study, the Z-scores of all the downregulated and upregulated genes were used. Finally, statistical models were developed for all the downregulated and upregulated genes, considering the Z-scores of all brain cancers; however, Z-scores were associated with P-values and were thus added to the P-value conversion scale.

*KM survival analysis*. Survival analysis provides a visual demonstration of the survival curves of ≥2 groups of biological organisms (34). In the present study, the PRECOG server dataset was used to develop KM survival plots and understand the survival of patients with different brain tumor subtypes. The KM survival plots of different genes were incorporated into the server as built-in properties. The developed KM plots were informed of the high- and low-risk groups, and the PRECOG dataset was used for the KM plot development of

Table I. Primers used in quantitative PCR.

| Gene | Primer (5'-3') | |
|---|---|---|
| | Forward | Reverse |
| TIE1 | CCCAGATTGCGCTACAGCTA | GCCCGCGTAAGTGAAGTTCT |
| CACNA2D1 | CTGACGGTCCAAATCCTTGT | GTCATAACAGGCGGTGTGTG |
| CAPN6 | ACTATGGGTCCTCCTCTG | AGCTGGTGGTTGCTAATG |
| ADAMTS6 | TACCATGGCCGCAAAGACAT | TCCTAGGCTGGAATCACGGT |
| SAA1 | CTGCAGAAGTGATCAGCG | ATTGTGTACCCTCTCCCC |
| SAA2 | CTGCAGAAGTGATCAGCA | ATTATATGCATTATCTCAGC |
| GDF15 | GTTAGCCAAAGACTGCCACTG | CCTTGAGCCCATTCCACA |
| USP26 | CGATGATATGCGGGTGTTAG | GTACCCAGTGCAACGCCTAT |
| GADPH | GACCCCTTCATTGACCTCAAC | CTTCTCCATGGTGGTGAAGA |

TIE1, tyrosine kinase with immunoglobulin and epidermal growth factor homology domains 1; CACNA2D1, calcium voltage-gated channel auxiliary subunit α2Δ1; CAPN6, calpain 6; ADAMTS6, a disintegrin and metalloproteinase with thrombospondin motifs 6; SA, serum amyloid; GDF15, growth differentiation factor 15; USP26, ubiquitin specific peptidase 26.

brain tumor subtypes. In certain cases, patient data for specific genes in specific brain tumors were not available. Therefore, it was not possible to develop these plots. KM plots were generated using all downregulated and upregulated genes from the dataset using meta-Z analysis.

*In silico gene expression pattern of downregulated and upregulated genes*. Gene expression patterns were assessed for all downregulated and upregulated genes. In the present study, the Genomic Data Commons-The Cancer Genome Atlas (TCGA) data (https://genome.ucsc.edu/) for 671 GBM samples were used for analysis. A gene expression plot was developed using the copy number of the genes and RNAseq-HTseq-FPKM-UQ data. The University of California Santa Cruz Cancer Genomics Browser was used (35). $Log_2$ transformed data were used for statistical analysis.

*Establishing a PPI network and cluster analysis of upregulated and downregulated genes*. First, the GeneCards database was searched for all upregulated and downregulated genes (36,37). In the present study, the PPI networks of the Search Tool for the Retrieval of Interacting Genes/Proteins (STRING) (https://string-db.org/) linked the respective genes. Using STRING, an interaction network was developed for all the upregulated and downregulated genes using the STRING server (StringApp version 1.7.1) (38). To develop the network, medium confidence (0.400) of the STRING server was used, and all other input parameters were set as general parameters. In the STRING server, no clustering was applied, and the network was shown as a network. Cluster analyses were performed using the STRING server using all upregulated and downregulated genes, which were identified in the NGS and quantitative (q)PCR analyses of the TMZ-resistant GBM8401 cell samples. Finally, the outcomes from the STRING tool were combined with those from the Cytoscape software (v. 3.9.1; https://cytoscape.org/) to establish the PPI network.

*Construction of a co-expression gene network and hierarchical clustering using all upregulated and downregulated genes*. A co-expression gene network and hierarchical clustering were constructed using the COXPRESdb v7 server (https://coxpresdb.jp/). All downregulated and upregulated genes [tyrosine kinase with immunoglobulin and epidermal growth factor homology domains 1 (*TIE1*), calcium voltage-gated channel auxiliary subunit α2Δ1 (*CACNA2D1*), calpain 6 (*CAPN6*) and a disintegrin and metalloproteinase with thrombospondin motifs 6 (*ADAMTS6*)] and upregulated [serum amyloid (*SA*)*A1*, *SAA2*, growth differentiation factor 15 (*GDF15*) and ubiquitin specific peptidase 26 (*USP26*)] were converted to Entrez Gene IDs (39). The Entrez Gene IDs of all genes were used as query sequences. In the present study, two types of co-expressed gene networks were developed. The first was a co-expressed gene plot using Entrez Gene IDs, which provided a global view of the network. The global view in two dimensions showed a co-expressed gene plot of the query genes. The second was a co-expressed gene plot with the query and co-expressed genes. Hierarchical clustering was also performed using all the upregulated and downregulated genes. The two server parameters used were *Homo sapiens* species and hsa-u. The c4-0 platform was used for analysis. These two parameters were selected in the COXPRESdb v7 server for the analysis.

*Samples collection*. Prior to the start of the present study, GBM (WHO Grades 3 and 4) samples from different surgeries were deposited into the tissue bank of Kaohsiung Chang Gung Memorial Hospital (Kaohsiung, Taiwan) as a general hospital procedure in March 2019, November 2020 and April 2021. Following approval from the Institutional Review Board, GBM samples were collected from the hospital tissue bank to initiate the study and perform further analysis, in accordance with the hospital's tissue bank regulations and other regulatory procedures. A total of two types of samples were collected from 6 patients: GBM with wild-type IDH or mutant IDH. The present study was approved by the Chang Gung

Medical Foundation Institutional Review Board (approval no. 201902218B1B0).

*Immunohistochemical staining*. Tissues were fixed in 4% paraformaldehyde at 4˚C overnight, and embedded in paraffin. Tissue blocks were sectioned at a thickness of 4 $\mu$m on slides. Tissue sections were deparaffinized in two changes of xylene, rehydrated in a graded series of ethanol and rinsed in distilled water. For antigen retrieval, the slides were incubated with proteinase K (cat. no. P2308, Sigma-Aldrich; Merck KGaA) in Tris-EDTA buffer for 45 min in a water bath at 37˚C, and endogenous peroxidases were quenched with 3% $H_2O_2$ in phosphate-buffered saline for 8 min at room temperature. The sections were blocked with 4% horse serum (cat. no. 008-000-121; Jackson ImmunoResearch Laboratories, Inc.) in 0.1% bovine serum albumin (cat. no. 01-000-161; Jackson ImmunoResearch Laboratories, Inc.) for 3 h at room temperature, followed by incubation with primary antibodies diluted in 2% horse serum (cat. no. 01-000-161; Jackson ImmunoResearch Laboratories, Inc.) overnight at 4˚C. The primary antibodies used were anti-SAA1 (1:100; cat. no. E-AB-52681; Elabscience Biotechnology, Inc.), anti-SAA2 (1:100; cat. no. 13192-1-AP; Proteintech Group, Inc.), anti-TIE1 (1:500; cat. no. ab111547; Abcam) and anti-Calpain 6 (1:100; cat. no. ab76974; Abcam). The sections were then incubated with biotinylated secondary antibodies (cat. no. BA-1100; Vector Laboratories, Inc.) diluted (1:400) in 2% horse serum (cat. no. 008-000-121; Jackson ImmunoResearch Laboratories, Inc.) for 90 min at room temperature. Signals were detected using an avidin-biotin complex (cat. no. PK-6100; Vector Laboratories, Inc.) and 3,3-diaminobenzidine tetrahydrochloride (cat. no. SK-4100; Vector Laboratories, Inc.). The images were captured using a light microscope (Leica DM 6000 B; Leica Microsystems GmbH) and Leica Application Suite X software (version: 5.1.0.25593; Leica Microsystems GmbH). Immunohistochemical analysis was performed as previously described (40,41). Immunohistochemical images were acquired at x200 magnification under the same exposure time and measured for each pixel value of the positive area using freely available ImageJ software version 1.53k (National Institutes of Health) without a specific plugin to perform deconvolution and downstream analysis. The images were analyzed using a region of interest manager to calculate the number of immunoreactive pixels occupied by the target protein. For each tissue specimen, three tissue fields were randomly selected and analyzed.

*Evaluation of the mutational landscape of IDH in GBM through in silico models*. Molecular modeling of the IDH structure was based on two published three-dimensional (3D) structures. A total of three types of structures were developed: i) Wild-type IDH, ii) IDH1 with mutation at position R132, iii) and IDH3 with mutation at positions R140 and R172. Structures from the Protein Data Bank (PDB; PDB ID: 3MAP, 3MAS and 1T09) were retrieved for further analysis (42). The modeled 3D structure of IDH was further analyzed using PyMOL 2.6 (43). Another 3D model of IDH was developed using AlphaFold 3.0 (44), and wild-type and mutant IDH structures were developed (positions R132, R140 and R172). The 3D model was validated using the same server. The secondary structural landscape was analyzed using PDBsum 2.58 (45).

*Statistical analysis*. The cell viability was analyzed using one-way analysis of variance and Dunnett's post-hoc test. The data of the immunohistochemical staining assay were analyzed using unpaired Student's t-tests. Statistical graphs, plots and models were constructed using the PAST 4.03 statistical software (46). This software built the 'statistical models' and depicted the 'polynomial models' order 2 with the $R^2$ value. In the present study, the 'statistical models/statistical plots' were developed using gene expression and other data. Simultaneously, MATLAB 9.6 was also used to analyze and depict the plots and graphs (47). For KM survival analysis, a median split was used by the PRECOG web server to generate KM plots, and the log-rank test was used by the server for curve separation.

An outline of the workflow of the present study is presented in Fig. 1, including the strategies and step-by-step analysis.

## Results

*Establishing a TMZ-resistant GBM cell line*. Drug resistance is a critical clinical issue in patients with cancer, resulting in therapeutic failure. TMZ, an imidazotetrazine, is an anticancer drug commonly used to treat patients with GBM; however, TMZ resistance is a common problem in GBMs (48). To assess TMZ resistance in TMZ-resistant GBM, a cell viability study was performed using MTT assays to determine the anticancer effects of different doses of TMZ in GBM8401 and TMZ-resistant GBM8401 cell lines for different periods (24, 48 and 72 h). The viability results of TMZ treatment in GBM8401 and TMZ-resistant GBM8401 cell lines from the MTT assay are presented in Fig. 2. After 48 h, treatment with 200 and 400 $\mu$M TMZ significantly reduced cell viability to ~80 and 70%, respectively, in comparison with cells treated with 0 $\mu$M TMZ. Similarly, it was demonstrated that treatment with 200 and 400 $\mu$M TMZ significantly reduced cell viability after 72 h to ~70 and 58%, respectively, in comparison with cells treated with 0 $\mu$M TMZ (Fig. 2A). Furthermore, in TMZ-resistant GBM8401, treatment with 400 $\mu$M TMZ significantly reduced cell viability to ~80% after both 48 and 72 h, in comparison with cells treated with 0 $\mu$M TMZ. However, no significant effect was observed after treatment with 200 $\mu$M TMZ after 48 or 72 h (Fig. 2B).

*NGS and qPCR analysis in TMZ-resistant GBM8401 cells*. Using NGS, two groups of GBM cells were analyzed: Normal and TMZ-resistant. The results revealed that, compared with the normal group, 20 genes were upregulated >2 times and 20 genes were downregulated >2 times in the TMZ-resistant group. The O6-methylguanine-DNA-methyltransferase (MGMT) gene has been upregulated in cases of resistance to the drug TMZ (49). As a result, this gene was intentionally omitted from the scope of this study. Further validation of NGS results was performed using qPCR. After analyzing NGS and qPCR, a focus was placed on the genes that showed a decrease of >2 times in expression (Table II) and those that showed an increase of >2 times in expression (Table III) in TMZ-resistant cells.

Downregulated (*TIE1, CACNA2D1, CAPN6* and *ADAMTS6*) and upregulated (*SAA1, SAA2, GDF-15* and *USP26*) genes were

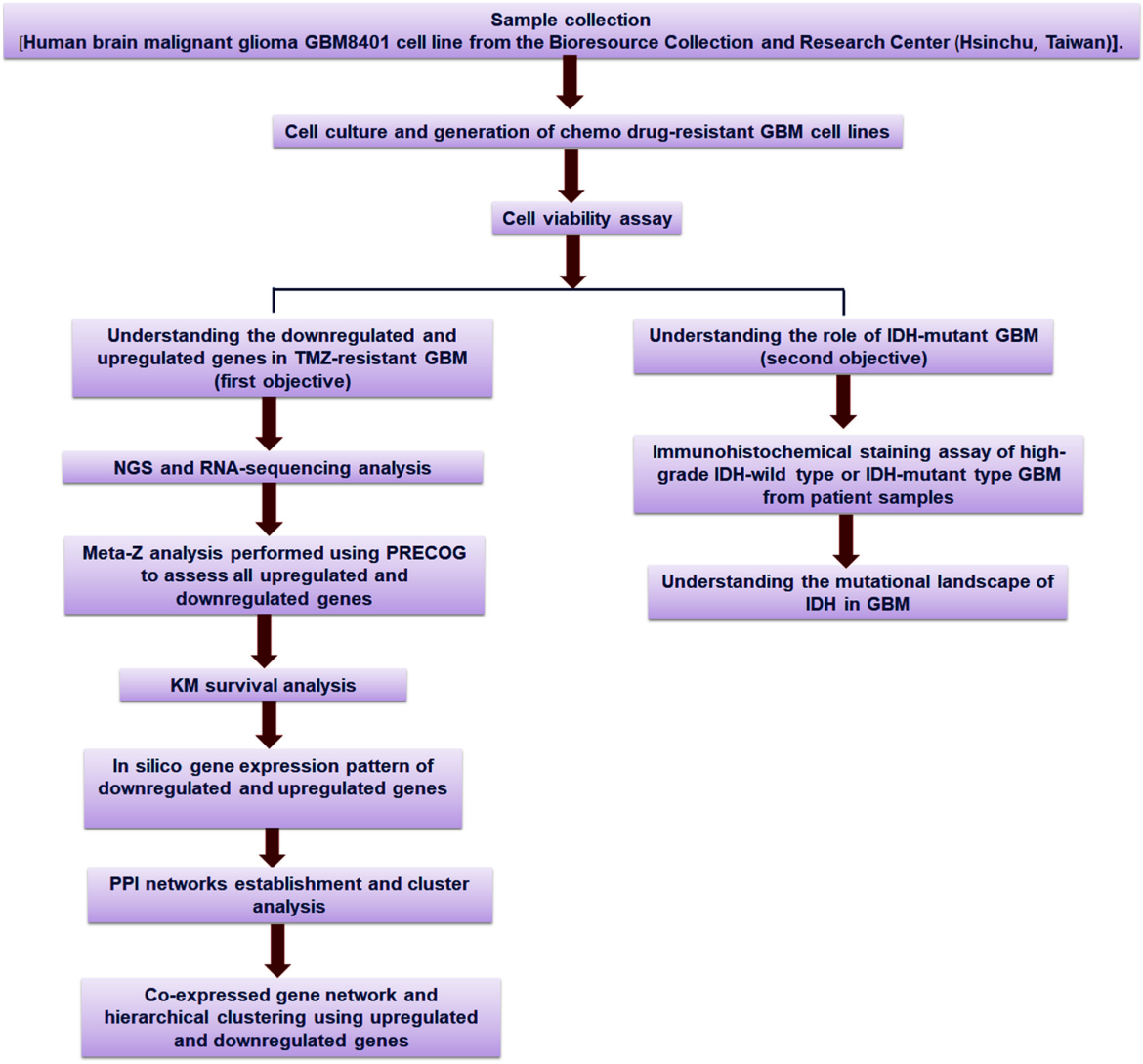


Figure 1. Schematic diagram of the overall study methodology. The study was performed with two objectives: First, it aimed to assess the downregulated and upregulated genes and their profiles using TMZ-resistant GBM cell lines; and second, it aimed to understand the mutational landscape of IDH in GBM. For the first objective, NGS and RNA-sequencing analyses, meta-Z analysis using PRECOG, KM survival analysis using PRECOG, *in silico* gene expression pattern analysis, PPI networks establishment and cluster analysis of the co-expressed gene network, and hierarchical clustering were performed. For the second objective, an immunohistochemical staining assay of the upregulated and downregulated genes in IDH-wild type or mutant cells as well as *in silico* analysis of the mutational landscape of IDH in GBM through several developed models were performed. TMZ, temozolomide; GBM, glioblastoma multiforme; IDH, isocitrate dehydrogenase; NGS, next-generation sequencing; PRECOG, Prediction of Clinical Outcomes from Genomic Profiles; KM, Kaplan-Meier; PPI, protein-protein interaction.

identified. A statistical model was developed to understand gene patterns using NGS data (Fig. 3A). *TIE1* had the greatest level of downregulation (-3.85766), whilst *CAPN6* had the least (-3.05983). Furthermore, *USP26* had the greatest level of upregulation (4.788689), whilst *SAA1* had the least (3.432643). The polynomial statistical model yielded an $R^2$ value of 0.4063.

Simultaneously, another statistical model was developed to identify the patterns of upregulated and downregulated genes using the qPCR data (Fig. 3B). According to this model, *TIE1* had the greatest level of downregulation (0.05), whilst *ADAMTS6* had the least (0.26). Furthermore, *SAA2* had the greatest level of upregulation (11.70), whilst USP26 had the least (3.94). The polynomial statistical model yielded an $R^2$ value of 0.3439.

*Meta-Z analysis of all upregulated and downregulated genes from TMZ-resistant GBM8401 cells using the PRECOG server.* Meta-Z analysis using the PRECOG server revealed the Z-scores of all the upregulated and downregulated genes. The Z-scores of the downregulated genes (*TIE1, CACNA2D1, CAPN6* and *ADAMTS6*) were determined for different types of brain cancer (Fig. 4). Z-scores indicate the survival outcomes for candidate genes. According to the correspondence table, Z-scores can be converted to P-values, Z-score >1.96, which is equivalent to P<0.05. In the present study, different statistical models of the downregulated genes (*TIE1, CACNA2D1, CAPN6* and *ADAMTS6*) in different brain cancers, such as astrocytomas, glioblastomas, gliomas, medulloblastomas, meningiomas and neuroblastomas, were developed (Fig. 5). For *TIE1*, the models demonstrated that the highest Z-score was for meningioma and the lowest was for astrocytomas (Fig. 5A). Similarly, for *CACNA2D1*, the models revealed that the highest Z-score was for neuroblastoma and the lowest for

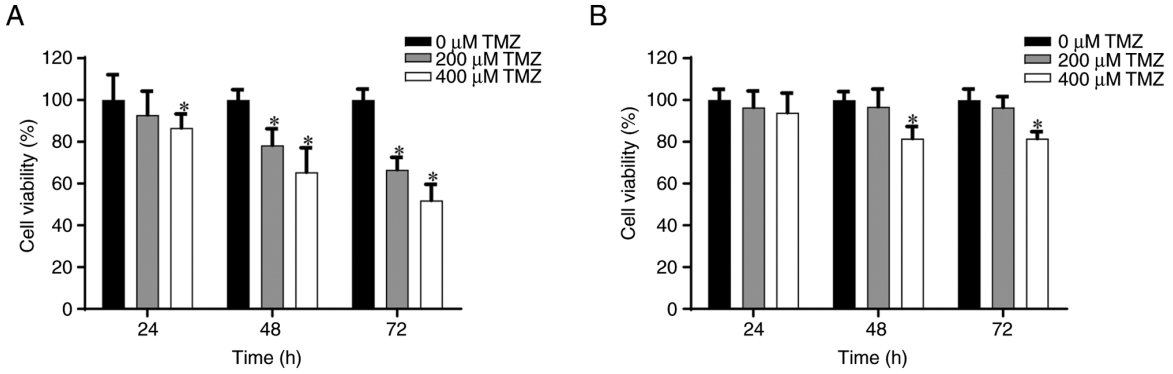


Figure 2. Cell viability of glioblastoma multiforme after TMZ treatment. Anticancer effect of TMZ on (A) GBM8401 and (B) TMZ-resistant GBM8401 cell lines after 24, 48 and 72 h. Values are expressed as the mean ± standard deviation. The data were analyzed using one-way analysis of variance and Dunnett's post-hoc test. *P<0.05 compared with the control. TMZ, temozolomide.

astrocytoma (Fig. 5B). For *CAPN6*, the highest Z-score from the developed models was for GBM and the lowest was for meningioma (Fig. 5C). Finally, for *ADAMTS6*, the statistical models demonstrated that the highest Z-score was for neuroblastomas and the lowest was for astrocytomas (Fig. 5D).

Similarly, the Z-scores of the upregulated genes (*SAA1, SAA2, GDF15* and *USP26*) were determined for different types of brain cancer (Fig. 4) and several statistical models were developed for these upregulated genes in the aforementioned types of brain cancer (Fig. 6). For *SAA1*, the models demonstrated that the highest Z-score was for neuroblastomas and the lowest was for astrocytomas (Fig. 6A). Similarly, for *SAA2*, the statistical models revealed that the highest Z-score was for neuroblastoma and the lowest was for GBM (Fig. 6B). Similarly, for *GDF15*, the statistical models demonstrated that the highest Z-score was for gliomas and the lowest was for medulloblastomas (Fig. 6C). Finally, for *USP26*, it was revealed that the highest Z-score was for astrocytomas and the lowest was for neuroblastomas (Fig. 6D).

*KM survival analysis for downregulated genes*. KM analysis was performed for all downregulated genes (*TIE1, CACNA2D1, CAPN6* and *ADAMTS6*) in the present study using a cohort of patients with different brain cancers. KM plots were constructed using a patient cohort with astrocytoma, GBM, glioma and medulloblastoma. For *TIE1*, in the cohort of patients with astrocytoma (n=154), a log-rank test result of P=0.061 and hazard ratio (HR)=0.745; the cohort of patients with GBM (n=90) demonstrated similar log-rank test results (P=0.051; HR=0.1006); the cohort of patients with glioma (n=50) revealed a log-rank test result of P=0.091 and HR=0.875; and the patient cohort with medulloblastoma (n=60) demonstrated log-rank test results of P=0.39 and HR=1.178 (Fig. S1A). For CACNA2D1, the patient cohort with astrocytoma (n=154) revealed a log-rank test result of P=0.00051 and HR=0.722; the patient cohort with GBM (n=39) demonstrated a log-rank test result of P=0.08 and HR=1.348; the patient cohort with glioma (n=50) revealed a log-rank test result of P=0.55 and HR=0.908; and the patient cohort with medulloblastoma (n=60) demonstrated a log-rank test result of P=0.22 and HR=0.675 (Fig. S1B). For *CAPN6*, the patient cohort with astrocytoma (n=154) revealed a log-rank test result of P=0.46 and HR=1.215; the patient cohort with GBM (n=39) demonstrated a log-rank test result of P=0.41 and HR=0.1.094; the patient cohort with glioma (n=50) had a log-rank test result of P=0.63 and HR=1.02; and the patient cohort with neuroblastoma (n=85) demonstrated a log-rank test result of P=0.91 and HR=1.139 (Fig. S1C). Finally, for ADAMTS6, the patient cohort with astrocytoma (n=154) revealed a log-rank test result of P=0.15 and HR=1.089; the patient cohort with GBM (n=39) demonstrated a log-rank test result of P=0.09 and HR=1.024; the patient cohort with glioma (n=136) revealed a log-rank test result of P=0.48 and HR=1.23; and the patient cohort with meningioma (n=60) demonstrated a log-rank test result of P=0.81 and HR=0.627 (Fig. S1D).

*KM survival analysis for upregulated genes*. KM analysis was performed for all upregulated genes (*SAA1, SAA2, GDF15,* and *USP26*) in cohorts of patients with different brain cancers. Using the cohorts of patients with glioma and neuroblastoma, KM plots were generated for *SAA1*. The patient cohort with glioma (n=50) demonstrated a log-rank test result of P=0.043 and HR=1.721. Similarly, the patient cohort with neuroblastoma (n=85) revealed a log-rank test result of P=0.85 and HR=1.239 (Fig. S2A). KM plots of SAA2 expression was generated using patient cohorts with GBM and medulloblastoma. The cohort with GBM (n=39) demonstrated a log-rank test result of P 0.62 and HR=0.96. The patient cohort with medulloblastoma (n=60) revealed a log-rank test result of P=0.11 and HR=1.404 (Fig. S2B). KM plots for *GDF15* was generated using patient cohorts with astrocytoma, GBM, glioma and medulloblastoma. The patient cohort with astrocytoma (n=154) revealed a log-rank test result of P=0.082 and HR=1.273; the patient cohort with GBM (n=39) demonstrated a log-rank test result of P=0.83 and HR=0.0976; the patient cohort with glioma (n=50) had a log-rank test result of P=0.00028 and HR=1.479; and the patient cohort with medulloblastoma (n=60) demonstrated a log-rank test result of P=0.57 and HR=1.224 (Fig. S2C). KM curves for *USP26* were generated using patient cohorts with astrocytomas, glioblastomas, GBM and meningiomas. The astrocytoma patient cohort (n=154) revealed a log-rank test result of P=0.0012 and HR=0.0699; the patient cohort with GBM (n=39) demonstrated a log-rank test result of P=0.035 and HR=1.103; the patient cohort with glioma (n=136) revealed a log-rank test result of P=0.91 and HR=1.256; and the patient

Table II. Downregulated mRNAs in temozolomide-resistant GBM8401 cells.

| Gene | Gene expression NGS result | qPCR result |
|---|---|---|
| TIE1 | -3.85766 | 0.05 |
| CACNA2D1 | -3.27131 | 0.17 |
| CAPN6 | -3.05983 | 0.20 |
| ADAMTS6 | -3.66361 | 0.26 |

TIE1, tyrosine kinase with immunoglobulin and epidermal growth factor homology domains 1; CACNA2D1, calcium voltage-gated channel auxiliary subunit α2Δ1; CAPN6, calpain 6; ADAMTS6, a disintegrin and metalloproteinase with thrombospondin motifs 6; NGS, next-generation sequencing; qPCR, quantitative PCR.

Table III. Upregulated mRNAs in temozolomide-resistant GBM8401 cells.

| Gene | Gene expression NGS result | qPCR result |
|---|---|---|
| SAA2 | 4.384488 | 11.70 |
| GDF15 | 3.957493 | 6.18 |
| SAA1 | 3.432643 | 6.13 |
| USP26 | 4.788689 | 3.94 |

SA, serum amyloid; GDF15, growth differentiation factor 15; USP26, ubiquitin specific peptidase 26; NGS, next-generation sequencing; qPCR, quantitative PCR.

cohort with meningioma (n=67) demonstrated a log-rank test result of P=0.47 and HR=0.901 (Fig. S2D).

*Gene expression patterns of downregulated genes*. In the present study, the expression patterns of downregulated genes (*TIE1, CACNA2D1, CAPN6* and *ADAMTS6*) were determined using the GDC TCGA dataset of 671 GBM samples. First, the expression of *TIE1* in GBM samples was assessed. In the generated scatter plot, most sample data points were plotted within 14.5-18 on the x-axis (RNAseq-HTseq-FPKM-UQ data). The plotted data revealed Pearson's ρ=-0.06216 (P=0.4291) and Spearman's rank ρ=-0.1551 (P=0.04734; Fig. 7A). Second, the gene expression pattern of *CACNA2D1* was determined in GBM samples. The scatter plot demonstrated that most sample data points were plotted within 12-17 on the x-axis. The plotted data revealed Pearson's ρ=-0.1629 (P=0.03716) and Spearman's ρ=-0.1452 (P=0.06366; Fig. 7B). Third, the gene expression pattern of *CAPN6* was assessed in GBM samples. The generated scatter plot demonstrated that most sample data points were plotted within 16-17.5 of the x-axis. The plotted data revealed Pearson's ρ=0.1882 (P=0.01582) and Spearman's rank ρ=0.08109 (P=0.3020; Fig. 7C). Fourth, the gene expression pattern of *ADAMTS6* was evaluated using GBM samples. The scatter plot demonstrated that most sample data points were plotted within 0-15.5 of the x-axis. The plotted data revealed Pearson's ρ=0.1305 (P=0.09577) and Spearman's rank ρ=0.1046 (P=0.1827; Fig. 7D).

*Gene expression pattern of upregulated genes*. The expression patterns of the upregulated genes (*SAA1, SAA2, GDF15* and *USP26*) were also identified using 671 GDC TCGA GBM samples. First, the gene expression pattern of *SAA1* was assessed in GBM samples. The scatter plot demonstrated that most sample data were plotted along the x-axis (0-14; RNAseq-Htseq-FPKM-UQ data). The plotted data revealed Pearson's ρ=0.06606 (P=0.4007) and Spearman's rank ρ=-0.002141 (P=0.9783; Fig. 8A). Second, the gene expression pattern of *SAA2* was assessed in GBM samples. The scatter plot demonstrated that most of the sample data were plotted within 7.5-20 on the x-axis (RNAseq-Htseq-FPKM-UQ data). The plotted data revealed Pearson's ρ=0.06701 (P=0.3939) and Spearman's rank ρ=-0.006710 (P=0.9320; Fig. 8B). Third, the gene expression pattern of *GDF15* was assessed in GBM samples. A scatter plot was constructed from the analysis, which indicated that most sample data points were plotted within 12-20 on the x-axis. The samples were also scattered. The plotted data revealed Pearson's ρ=0.1229 (P=0.1170) and Spearman's rank ρ=0.06775 (P=0.3887; Fig. 8C). Finally, the gene expression patterns of *USP26* were determined using the same aforementioned samples. The scatter plot illustrated that there were fewer of these gene samples than the others, and the sample data were plotted within 6-9 on the x-axis. The plot revealed Pearson's ρ=0.02669 (P=0.7344) and Spearman's rank ρ=0.02925 (P=0.7101; Fig. 8D).

*Establishing a PPI network and cluster analysis using all upregulated and downregulated genes*. The physical and functional relationships between the proteins of the upregulated and downregulated genes were assessed. Several *in silico* analyses were performed to understand the characteristics of upregulated and downregulated protein coding genes by establishing a PPI network. The interactions within the PPI network of downregulated protein-coding genes (*TIE1, CACNA2D1, CAPN6* and *ADAMTS6*) were depicted using Cytoscape (Fig. 9A-D), which demonstrated that other proteins were associated with this network. In the PPI network for downregulated genes, the nodes denoting the proteins participated in the interactions which denote the protein coding genes. The edge of the network, which is part of the PPI network of two nodes, was also noted and shows the interactions between the two proteins. The maximum number of nodes in the PPI network was observed for *ADAMTS6* (n=23) and *TIE1* (n=23). The lowest number of nodes was observed in the PPI network of *CACNA2D1* (n=16). The maximum number of edges in the PPI network was observed for *CACNA2D1* (n=101), and the minimum number of edges was observed for *CAPN6* (n=41; Table SI). The results of the present study indicated that the PPI networks of *TIE1*, *CACNA2D1*, CAPN6 and *ADAMTS6* showed interactions between 6, 14, 7 and 2 partner proteins, respectively (Table SII). Simultaneously, a box plot was generated using the numbers of nodes and edges, where the number of edges was markedly greater than that of the nodes (Fig. 9E). The protein clusters of the downregulated genes assessed using the STRING server are also presented in Fig. S3.

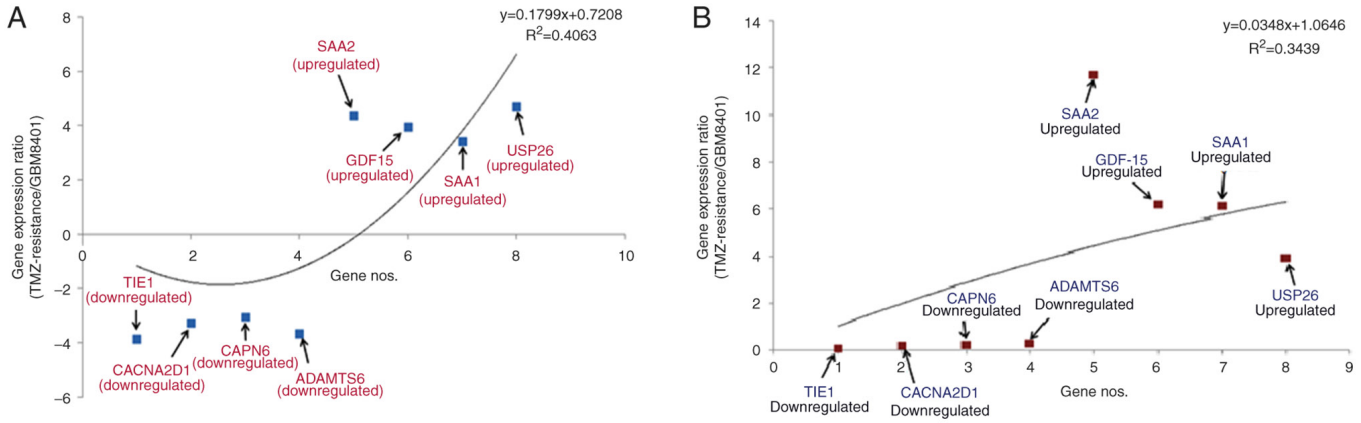


Figure 3. Pattern of differential gene expression in TMZ-resistant GBM8401 cells. Statistical model of upregulation and downregulation of the genes using (A) NGS and (B) qPCR data. TMZ, temozolomide; NGS, next-generation sequencing; qPCR, quantitative PCR; SAA2, serum amyloid A2; GDF15, growth/differentiation factor 15; SAA1, serum amyloid A1; USP26, ubiquitin-specific protease 26; TIE1, tyrosine kinase with immunoglobulin and epidermal growth factor homology domains 1; CACNA2D1, calcium voltage-gated channel auxiliary subunit α2Δ1; CAPN6, calpain 6; ADAMTS, a disintegrin and metalloproteinase with thrombospondin motifs 6.

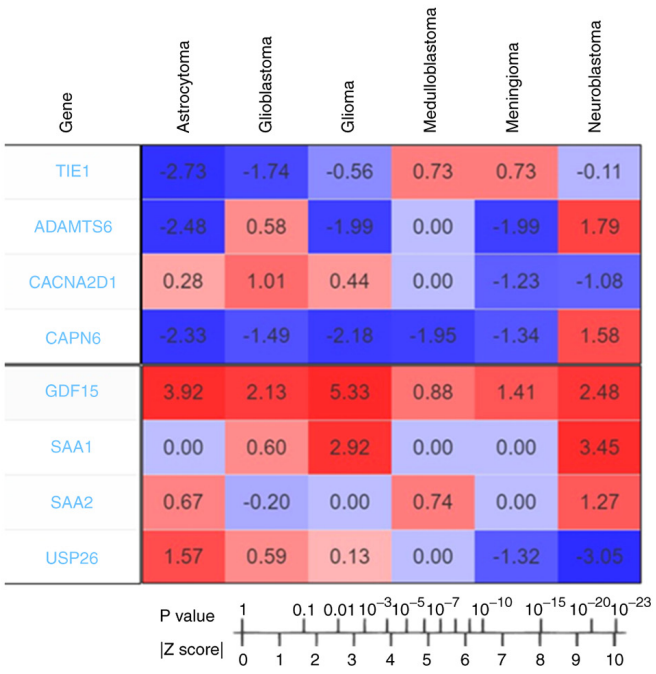


Figure 4. Outcomes of PRECOG analysis of downregulated (*TIE1*, *ADAMTS6*, *CACNA2D1* and *CAPN6*) and upregulated candidate genes (*GDF15*, *SAA1*, *SAA2* and *USP26*). The Z-scores represent the association between candidate genes and prognosis and are associated with P-values. The Z-score to P-value conversion was also recorded. The Z-scores indicate the survival outcome for candidate genes. The values indicating poor prognosis genes are shown in red, and those indicating good prognosis genes are shown in blue. This figure was generated using the PRECOG server. PRECOG, Prediction of Clinical Outcomes from Genomic Profiles; TIE1, tyrosine kinase with immunoglobulin and epidermal growth factor homology domains 1; CACNA2D1, calcium voltage-gated channel auxiliary subunit α2Δ1; CAPN6, calpain 6; ADAMTS6, a disintegrin and metalloproteinase with thrombospondin motifs 6; SA, serum amyloid; GDF15, growth differentiation factor 15; USP26, ubiquitin specific peptidase 26.

Furthermore, the PPI network proteins of the upregulated genes were established (Fig. 10A-D). Several other proteins associated with this network were also identified. In addition, the maximum number of nodes in the PPI network was identified for *USP26* (n=26) and the minimum number of nodes for *GDF15* (n=17). Moreover, the maximum number of edges in the PPI-network was reported for *SAA2* (n=236) and the minimum number of edges for *GDF15* (n=24; Table SI). The results of the present study indicated that the PPI network of *SAA1*, *SAA2*, *GDF15* and *USP26* showed interactions between 15, 21, 4 and 5 partner proteins, respectively (Table SII). Simultaneously, a box plot was developed using the number of nodes and edges (Fig. 10E). The number of edges is higher than the number of nodes; however, the range of the number of edges in the upregulated genes is greater than that in the downregulated genes. Protein clusters of downregulated genes identified using the STRING server are also present (Fig. S4).

*Establishing a PPI network using all upregulated and downregulated genes as a whole*. Finally, a PPI network was established using all downregulated and upregulated genes as input samples (Fig. 11A). The PPI network contained 35 nodes and 241 edges (Table SI). Furthermore, a bar diagram was generated to demonstrate the numbers of nodes and edges assessed using a statistical model (Fig. 11B). For the polynomial statistical model, the $R^2$ value was 1.297.

*Co-expressed gene network and hierarchical clustering*. In the present study, a co-expressed gene network was described. The Entrez Gene IDs of all downregulated and upregulated genes were used as inputs or query genes (Table SIII). First, a plot of co-expressed genes was constructed. This provided a global view of the two-dimensional form of the network. The global co-expressed gene plot demonstrated that only 4/8 query genes (*TIE1*, *CAPN6*, *SAA1* and *GDF15*) were involved in generating the co-expressed gene plot (Fig. 12A). Additionally, the co-expressed gene plot with the query and co-expressed genes revealed that several co-expressed genes were involved in co-expressed gene plot generation (Fig. 12B).

Hierarchical clustering of a co-expressed gene network of all downregulated and upregulated genes was performed. Hierarchical clustering is represented by a heat map in Fig. 12C. Hierarchical clustering of the co-expressed gene network revealed

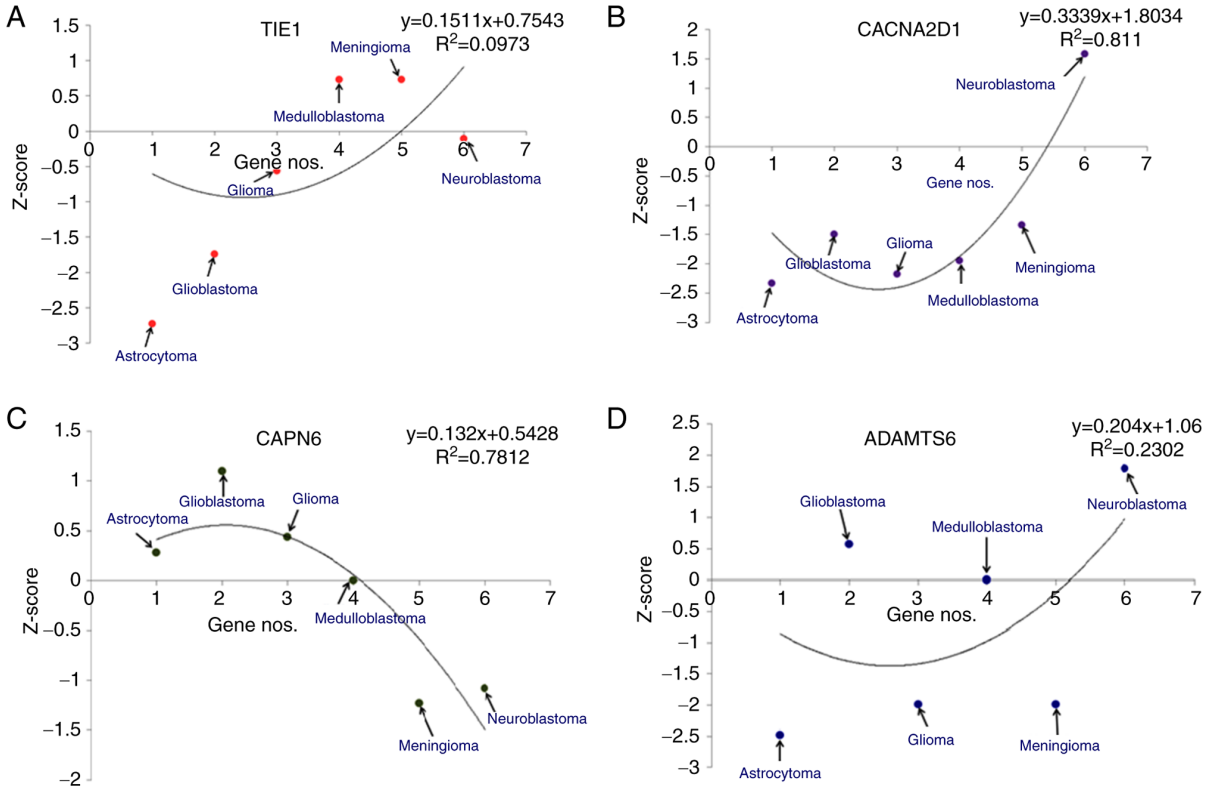


Figure 5. Different statistical models of downregulated genes in different types of brain cancer, such as astrocytoma, glioblastoma, glioblastoma multiforme, medulloblastoma, meningioma and neuroblastoma. The Z-scores of downregulated genes are shown: (A) *TIE1*, (B) *CACNA2D1*, (C) *CAPN6* and (D) *ADAMTS6*. TIE1, tyrosine kinase with immunoglobulin and epidermal growth factor homology domains 1; CACNA2D1, calcium voltage-gated channel auxiliary subunit α2Δ1; CAPN6, calpain 6; ADAMTS6, a disintegrin and metalloproteinase with thrombospondin motifs 6.

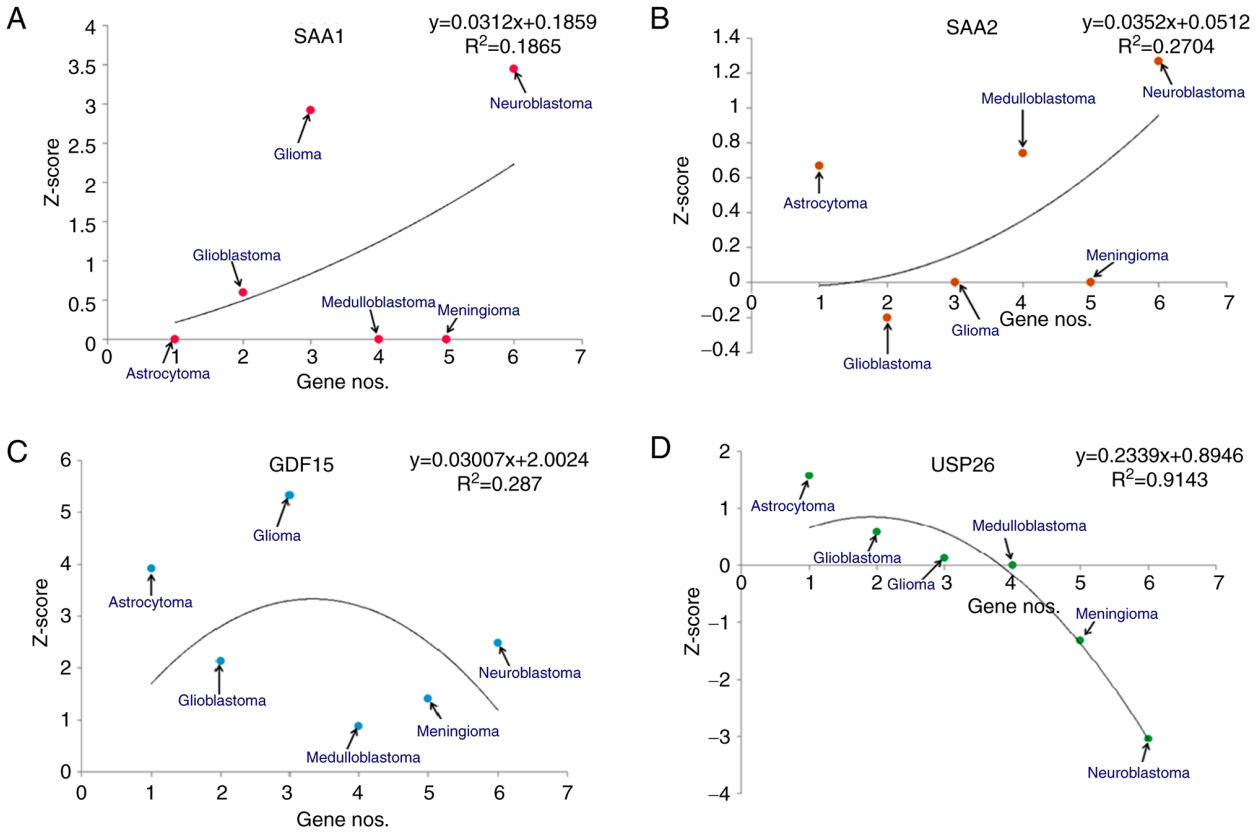


Figure 6. Different statistical models of upregulated genes for different types of brain cancer such as astrocytoma, glioblastoma multiforme, glioma, medulloblastoma, meningioma and neuroblastoma. The Z-scores of upregulated genes are shown: (A) *SAA1*, (B) *SAA2*, (C) *GDF15* and (D) *USP26*. SA, serum amyloid; GDF15, growth differentiation factor 15; USP26, ubiquitin specific peptidase 26.

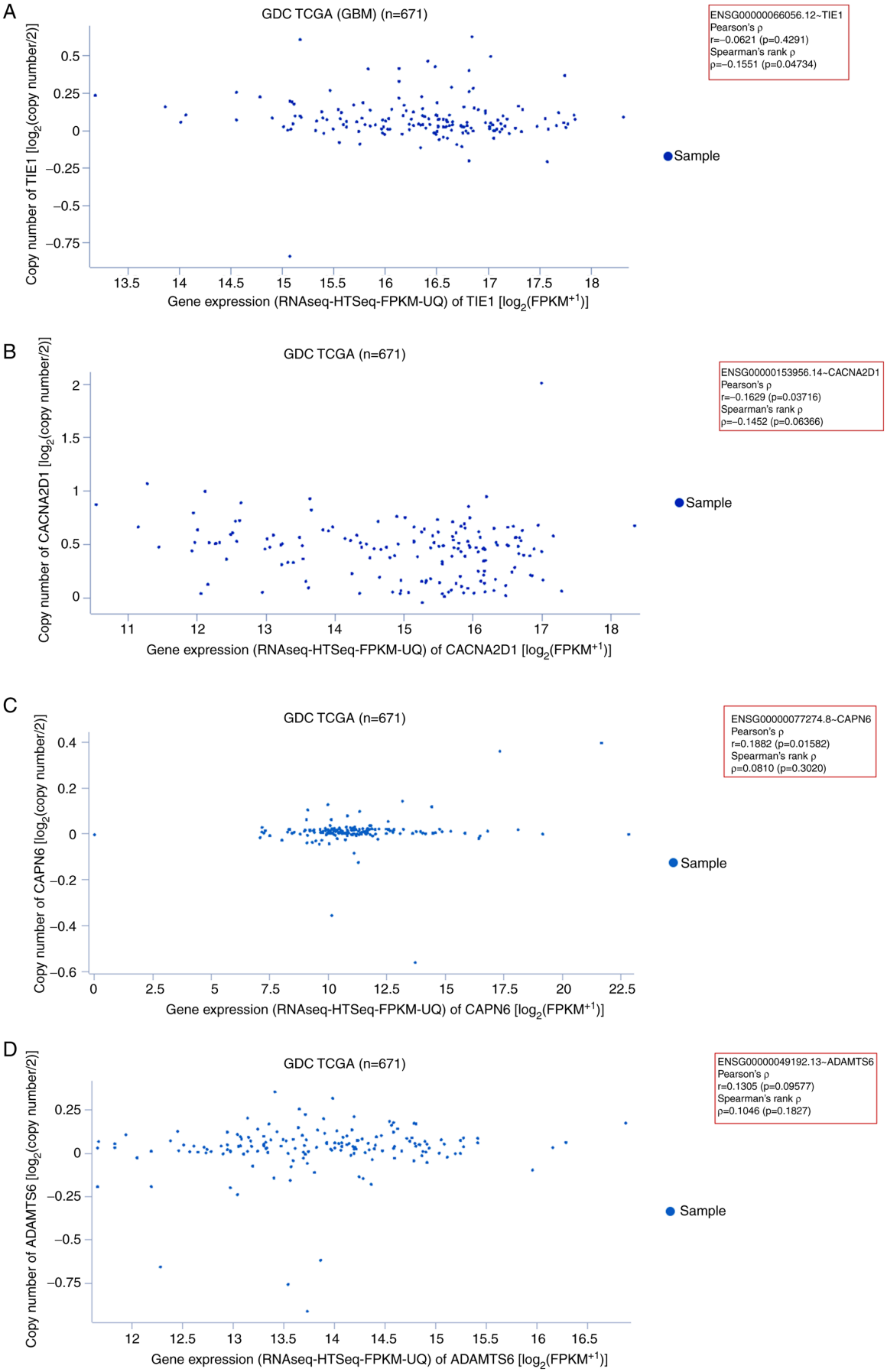


Figure 7. Gene expression pattern of downregulated genes assessed using 671 GDC TCGA GBM samples and represented through scatter plots. Gene expression pattern of (A) *TIE1*, (B) *CACNA2D*, (C) *CAPN6* and (D) *ADAMTS6* in GBM samples. GDC TCGA, Genomic Data Commons-The Cancer Genome Atlas; GBM, glioblastoma multiforme; TIE1, tyrosine kinase with immunoglobulin and epidermal growth factor homology domains 1; CACNA2D1, calcium voltage-gated channel auxiliary subunit α2Δ1; CAPN6, calpain 6; ADAMTS6, a disintegrin and metalloproteinase with thrombospondin motifs 6.

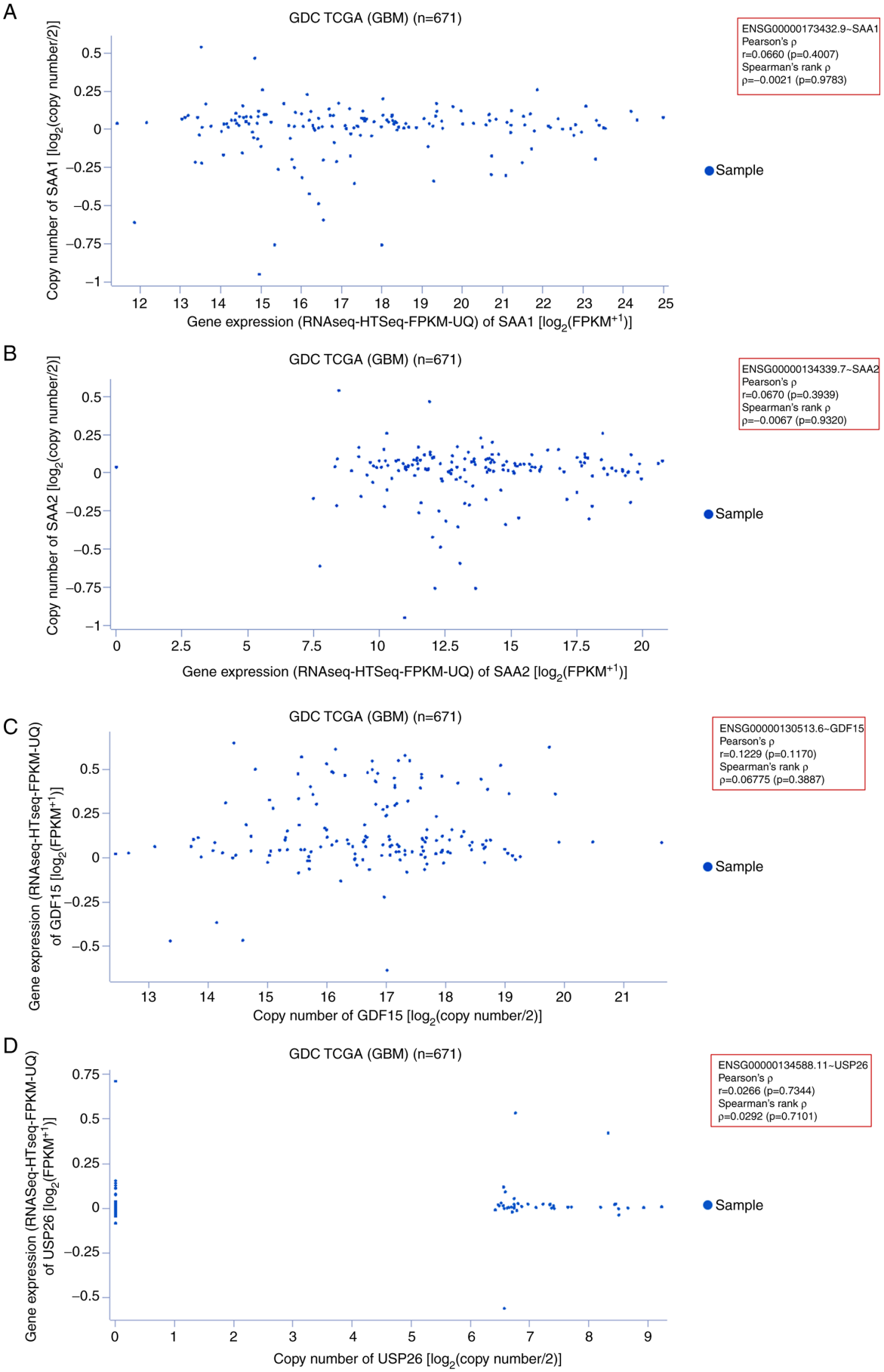


Figure 8. Gene expression pattern of the upregulated genes assessed using 671 GDC TCGA GBM samples and represented through scatter plots. Gene expression pattern of (A) *SAA1*, (B) *SAA2*, (C) *GDF15* and (D) *USP26* using GBM samples. GDC TCGA, Genomic Data Commons-The Cancer Genome Atlas; GBM, glioblastoma multiforme; SA, serum amyloid; GDF15, growth differentiation factor 15; USP26, ubiquitin specific peptidase 26.

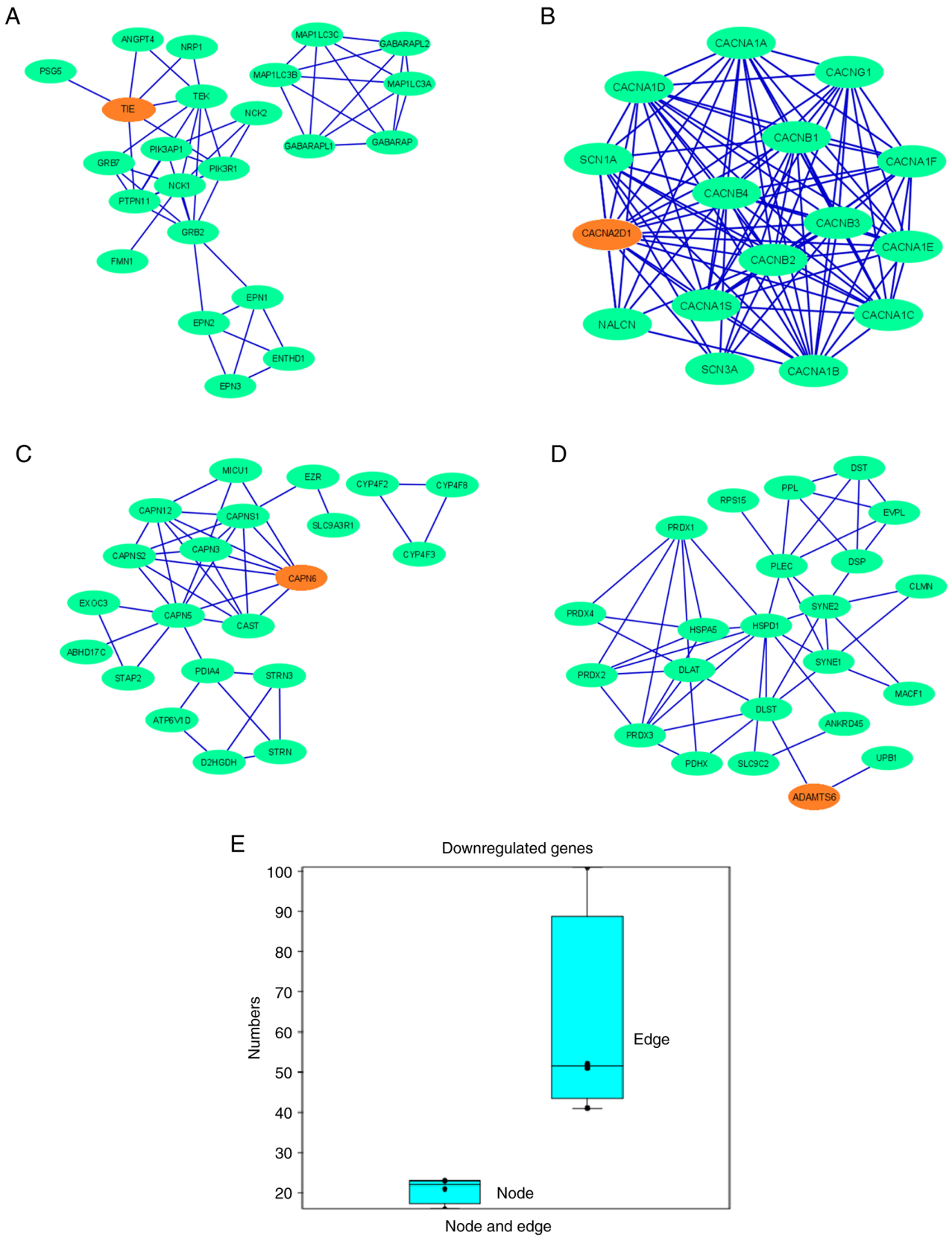


Figure 9. PPI network demonstrates the PPIs of the protein-coding downregulated genes depicted using Cytoscape. Nodes are represented as green elliptical shapes. Edges are represented by blue lines. PPI network demonstrates the PPIs of the protein-coding gene (A) *TIE1*, showing two clusters in the PPI networks. One main cluster has two sub-clusters, with one demonstrating no interactions with the gene of interest. The PPI network has 23 nodes and 52 edges; (B) *CACNA2D1*, showing one cluster in the PPI networks. The PPI network has 16 nodes and 101 edges; (C) *CAPN6*, showing two clusters in the PPI networks. One main cluster has two sub-clusters, with one demonstrating no interactions with the gene of interest. The PPI network has 21 nodes and 41 edges; and (D) *ADAMTS6*, showing one cluster of the PPI network. The PPI network has 23 nodes and 51 edges. (E) Box plot representing the number of nodes and edges of all the downregulated genes. PPI, protein-protein interaction; TIE1, tyrosine kinase with immunoglobulin and epidermal growth factor homology domains 1; CACNA2D1, calcium voltage-gated channel auxiliary subunit α2Δ1; CAPN6, calpain 6; ADAMTS6, a disintegrin and metalloproteinase with thrombospondin motifs 6.

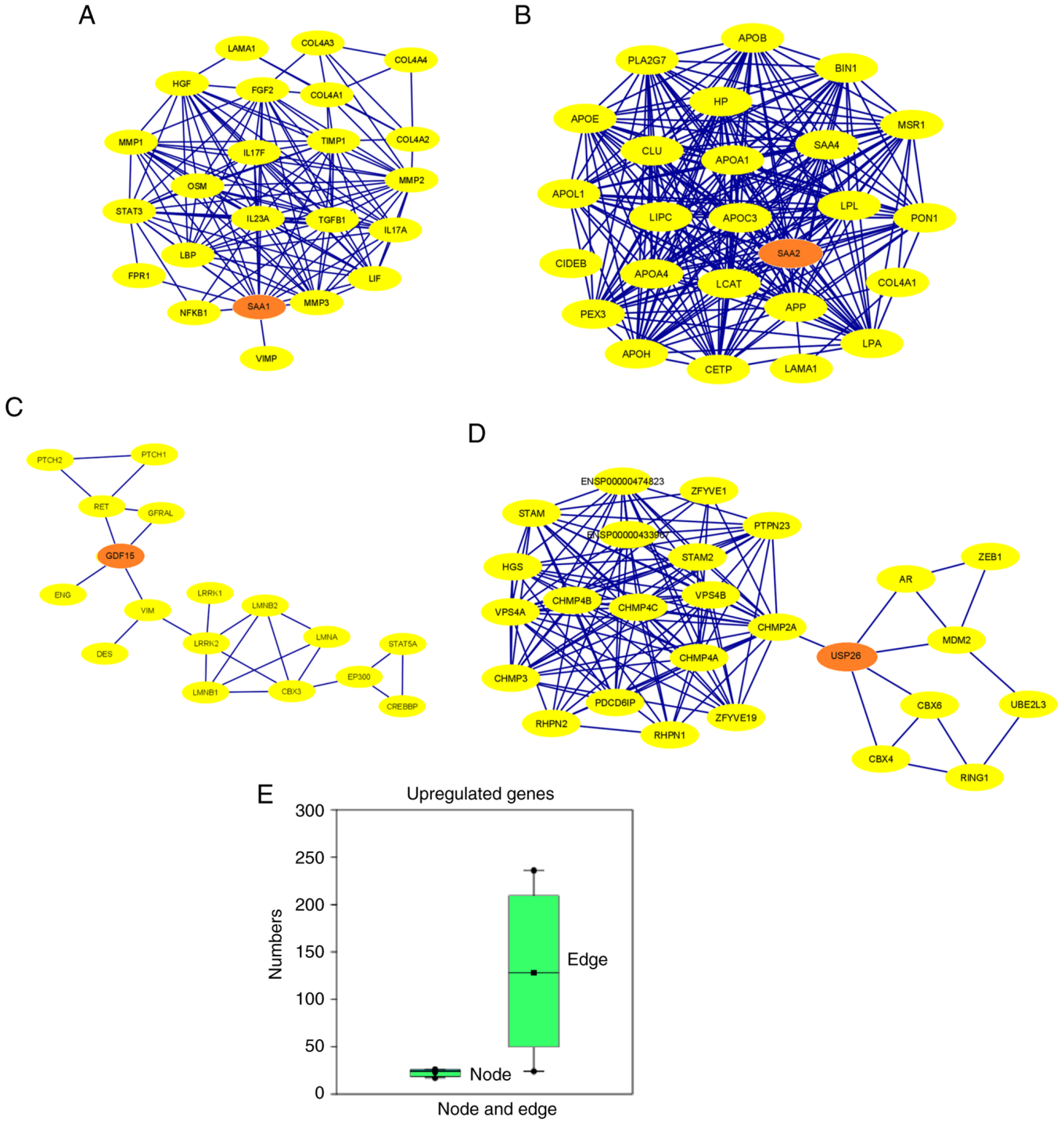


Figure 10. PPI network demonstrates the PPI of the protein-coding upregulated genes depicted using Cytoscape. Nodes are represented as yellow elliptical shapes. Edges are represented as blue lines. PPI network demonstrated the PPI of the protein-coding gene (A) *SAA1*, showing one cluster in the PPI network. The PPI network had 23 nodes and 129 edges; (B) *SAA2*, showing one cluster in the PPI network. This is the densest network among the upregulated genes. The PPI network has 25 nodes and 236 edges; (C) *GDF15*, showing one cluster in the PPI network. It is linear in shape and the lightest network among upregulated genes. The PPI network has 17 nodes and 24 edges; and (D) *USP26*, showing two clusters in the PPI network. The PPI network has 26 nodes and 127 edges. (E) Box plot representing the number of nodes and edges of all the upregulated genes. PPI, protein-protein interaction; SA, serum amyloid; GDF15, growth differentiation factor 15; USP26, ubiquitin specific peptidase 26.

a cluster of four genes: *TIE1*, *CAPN6*, *SAA1* and *GDF15*. Among these, two genes were upregulated and two were downregulated.

*Immunohistochemical staining assay to assess the upregulated and downregulated genes in IDH-wild type or mutant samples and their associations*. Immunohistochemical staining of GBM cells with wild-type or mutant IDH was performed. Immunohistochemical staining of IDH wild-type or IDH-mutant GBM samples with two downregulated mRNA-encoded proteins (TIE1 and CAPN6) is presented in Fig. 13, and immunohistochemical staining of IDH-wild-type or IDH-mutant GBM samples of two upregulated mRNA-encoded

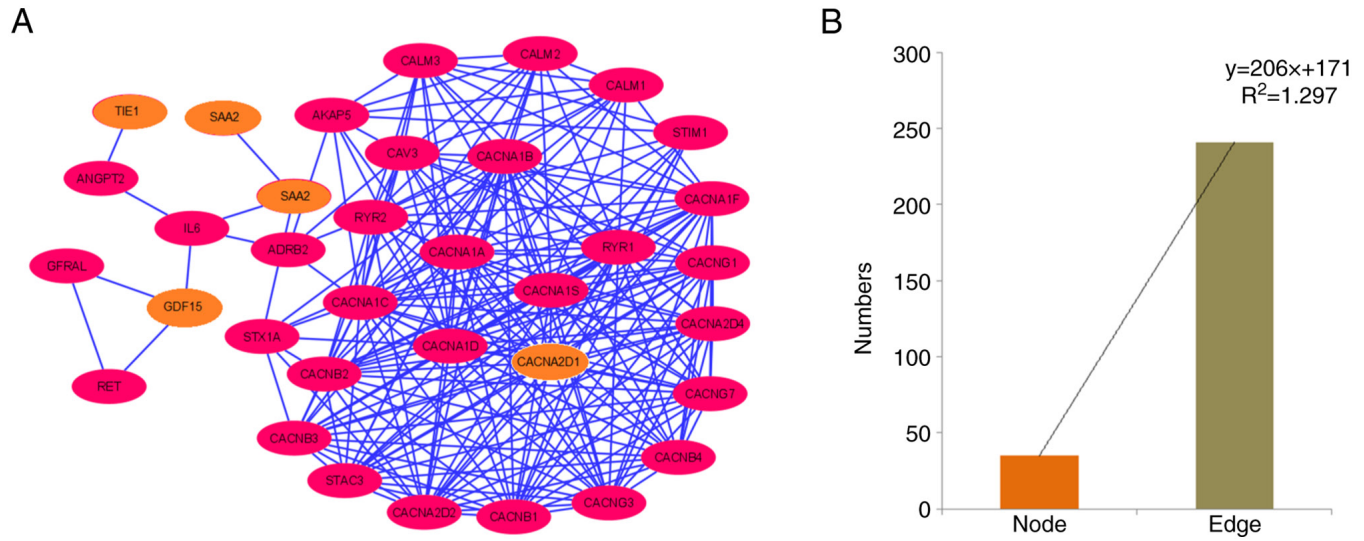


Figure 11. PPI network of the protein-coding downregulated and upregulated genes. (A) PPI network demonstrating the PPI of protein-coding downregulated and upregulated genes (*TIE1*, *CACNA2D1*, *CAPN6*, *ADAMTS6*, *SAA2*, *GDF15*, *SAA1*, and *USP26*), depicted using Cytoscape. Nodes are represented as pink elliptical shapes. Edges are represented as blue lines. A total of one cluster is shown in the PPI network. The PPI network has 35 nodes and 241 edges. (B) Bar diagram representing the number of nodes and edges of the PPI network. PPI, protein-protein interaction; TIE1, tyrosine kinase with immunoglobulin and epidermal growth factor homology domains 1; CACNA2D1, calcium voltage-gated channel auxiliary subunit α2Δ1; CAPN6, calpain 6; ADAMTS6, a disintegrin and metalloproteinase with thrombospondin motifs 6; SA, serum amyloid; GDF15, growth differentiation factor 15; USP26, ubiquitin specific peptidase 26.

proteins (SAA1 and SAA2) is demonstrated in Fig. 14. There was a significant upregulation of TIE1 (P<0.001) and CAPN6 (P<0.05) protein expression in IDH-mutant GBM compared with that in IDH wild-type (Fig. 13). Furthermore, there was a significant downregulation of SAA1 (P<0.001) and SAA2 (P<0.05) protein expression in IDH-mutant GBM compared with that in IDH wild-type (Fig. 14).

*Mutational landscape of IDH in GBM through in silico models.* The present study demonstrated the mutational landscape of IDH in GBM using *in silico* models. A total of three types of structures were developed through the molecular modeling of wild-type IDH: IDH1 with mutation position R132, and IDH2 with mutation position R140 or R172. Fig. 15A presents the wild-type IDH1 homodimer; Fig. 15B demonstrates the mutant-type IDH1, in which the mutated residue position R132 was identified; Fig. 15C illustrates the mutant-type IDH2, with mutation residue positions R140 or R172. Simultaneously, a secondary structural landscape of IDH was demonstrated. The mutated residue positions were indicated as R132 or R140 (Fig. 15D), demonstrating the position of the mutations in the alpha helices or beta sheets. In addition, a 3D structural model was developed using AlphaFold (Fig. 15E). Simultaneously, all three mutant residues (R132, R140 and R172) were identified in the model (3D model of the AlphaFold; Fig. 15F). Furthermore, the performance of the 3D structural model was validated using the aligned residues, and an expected position error was noted (Fig. 15G). Model performance evaluation using the aligned residues indicated that the model was significant.

Finally, the role of IDH mutations in GBM was illustrated (Fig. 16). The wild-type heterodimer exhibited regular IDH activity and could generate α-KG from isocitrate. The one-part mutant IDH heterodimer (wild-type/R132H) could generate D-2HG from α-KG. However, both one-part mutant types of the IDH heterodimer were inactive against IDH. Furthermore, IDH mutations were acquired by IDH, which resulted in considerable metabolic reprogramming. Neomorphic activity may diminish the Krebs cycle by draining α-KG for D-2-HG production. However, further studies are needed to confirm this hypothesis.

## Discussion

In the present study, experimental and *in silico* analyses were performed to assess the upregulated and downregulated genes in a GBM8401 resistant strain to fulfill two objectives: i) To establish the downregulated and upregulated genes and their profiles (characterized dysregulation); and ii) to understand the mutational landscape of IDH in GBM. To fulfill the first objective, both experimental and *in silico* analyses were used to evaluate the genes downregulated (*TIE1*, *CACNA2D1*, *CAPN6* and *ADAMTS6*) and upregulated (*SAA1*, *SAA2*, *GDF15* and *USP26*). First, the gene expression of TMZ-resistant GBM8401 cells was analyzed using NGS, and RNA expression profiles were assessed to determine the downregulated and upregulated genes. Meta-Z analysis was also performed using PRECOG to identify all the upregulated and downregulated genes in TMZ-resistant GBM. KM survival analysis, *in silico* gene expression pattern identification, PPI network establishment, cluster analysis of the co-expressed gene network, and hierarchical clustering of all upregulated and downregulated genes were performed. To fulfill the second objective, an immunohistochemical staining assay of high-grade GBM tissue with wild-type or mutant IDH from patient samples was performed. Finally, based on NGS analysis and qPCR data in TMZ-resistant GBM8401 cells, IDH-mutant GBM was compared with IDH wild-type

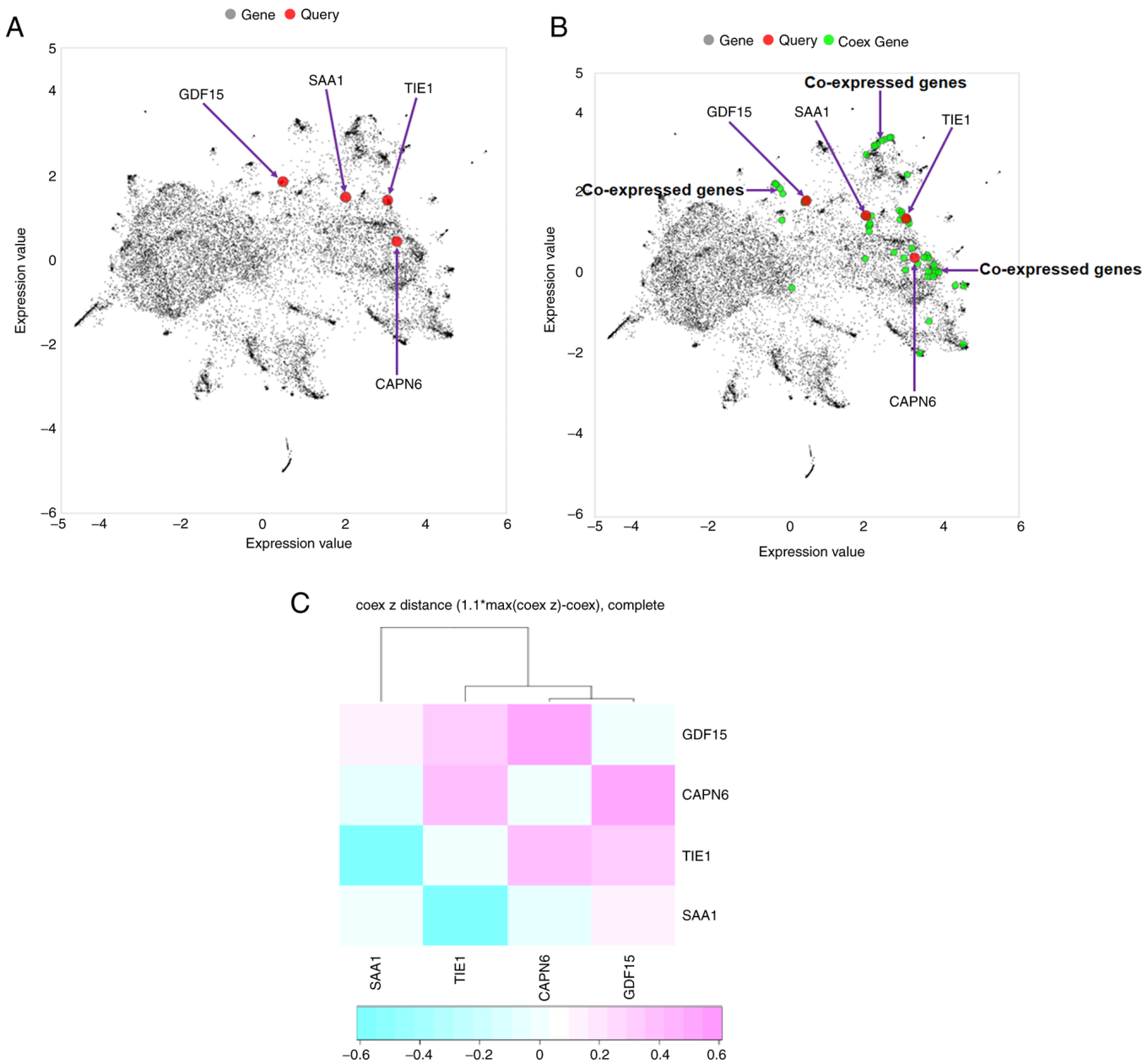


Figure 12. Co-expressed gene plot and hierarchical clustering. (A) Four query genes (*TIE1*, *CAPN6*, *SAA1* and *GDF15*) were found to be involved in generating a co-expressed gene plot. (B) Co-expressed gene plot with query and co-expressed genes. Several co-expressed genes were found in the plot. (C) Hierarchical clustering of the co-expressed gene network was developed using all downregulated and upregulated genes. The genes (*TIE1*, *CAPN6*, *SAA1* and GDF15) were found to be involved in the generation of hierarchical clustering. The Entrez Gene IDs of all downregulated and upregulated genes were used as input or query genes (*TIE1*, *CACNA2D1*, CAPN6, *ADAMTS6*, *SAA1*, *SAA2*, *GDF15* and *USP26*). TIE1, tyrosine kinase with immunoglobulin and epidermal growth factor homology domains 1; CACNA2D1, calcium voltage-gated channel auxiliary subunit α2Δ1; CAPN6, calpain 6; ADAMTS6, a disintegrin and metalloproteinase with thrombospondin motifs 6; SA, serum amyloid; GDF15, growth differentiation factor 15; USP26, ubiquitin specific peptidase 26; Coex, co-expressed.

GBM in terms of upregulated and downregulated genes. For comparison, two upregulated (*SAA1* and *SAA2*) and two downregulated genes (*TIE1* and *CAPN6*) were selected. The relative intensities of the expressed genes were determined in wild-type and mutant IDH cells. Finally, using *in silico* models, the present study illustrated the mutational landscape of IDH in GBM. Therefore, comprehensive, in-depth and step-by-step analyses were performed to elucidate the gene expression profile and pattern in GBM8401-resistant cells and the mutational landscape of IDH in GBM.

Chemotherapy resistance is a major global concern, with >90% of cancer-related deaths associated with MDR (50). Studies have focused on analyzing the gene expression patterns in chemotherapy-resistant cancers and the identification of differentially upregulated and downregulated genes in different cancers is a priority. For example, Rapin *et al* (51) compared the gene expression profiles of patients with acute myeloid leukemia, and recently, Cheng *et al* (52) investigated upregulated and downregulated genes in TMZ-resistant GBM cells. In the present study, upregulated and downregulated genes in TMZ-resistant GBM samples from hospitalized patients (TMZ-resistant GBM8401 cells) were analyzed. Therefore, the findings of the present study are important from the perspective of chemoresistance.

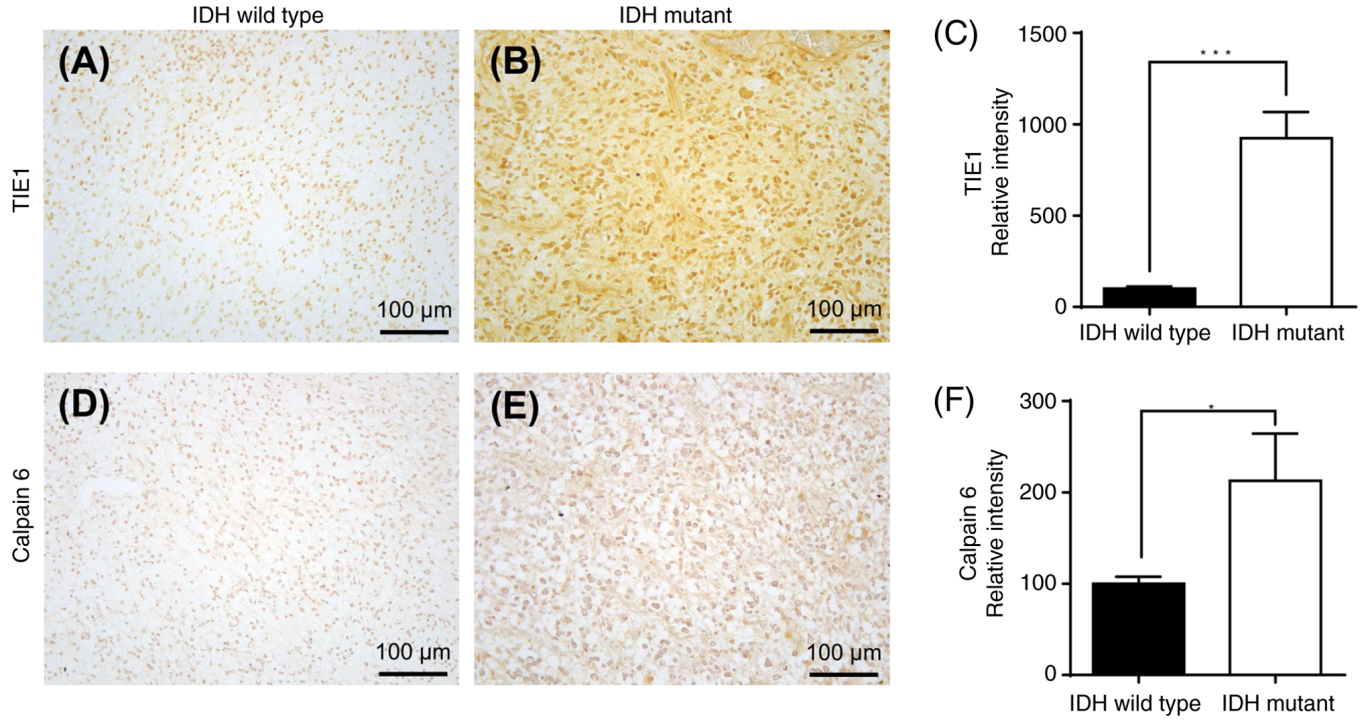


Figure 13. Immunohistochemical staining for TIE1 and CAPN6 expression on human GBM samples with either wild-type or mutant IDH. Representative images of TIE1-immunoreactivity in GBM tissues with (A) IDH wild-type and (B) IDH mutant. (C) TIE1 relative intensity in IDH wild-type and IDH-mutant samples. Representative images of CAPN6-immunoreactivity in GBM tissues with (D) IDH wild-type and (E) IDH-mutant. (F) CAPN6 relative intensity in IDH wild-type and mutant samples. Values are expressed as the mean ± standard deviation. The data were analyzed using unpaired Student's t-tests. $^{*}$P<0.05; $^{***}$P<0.001. IDH, isocitrate dehydrogenase; IHC, immunohistochemistry; TIE1, tyrosine kinase with immunoglobulin and epidermal growth factor homology domains 1; CAPN6, calpain 6.

Several researchers have used methods similar to those used in the present study to map gene expression in different types of cancer (53,54). In the present study, different *in silico* methods were used to understand the gene expression patterns in different types of brain cancer using the PRECOG server, and the Z-scores of the downregulated and upregulated genes were calculated. However, in addition to GBM, meta-Z analysis was performed for different types of brain cancers, such as astrocytoma, glioma, medulloblastoma, meningioma and neuroblastoma, for all upregulated and downregulated genes. The results of the present study provide further understanding of the prognostic landscape of genes in all human cancers. In addition, KM survival analysis was performed for different brain cancer types along with GBM. The observations from the analyses performed in the present study provide further understanding of the survival of patients with brain tumors.

Kothari *et al* (55) applied the PRECOG method to evaluate the Z-scores of genes in triple-negative breast cancer, which were analyzed using machine learning. Gentles *et al* (33) applied the PRECOG method to pan-cancer gene signatures related to cancer-associated fibroblasts. The present study attempted to identify the therapeutic targets. A PPI network was developed and cluster analysis was performed using the STRING server and Cytoscape software to depict the network between genes. Kumar *et al* (56) used the STRING server and Cytoscape software to develop a network of genes associated with ovarian cancer. Chakraborty *et al* (57) used the STRING server and Cytoscape software to map and create a network of immune protective genes against severe acute respiratory syndrome-coronavirus 2 infection. Similarly, studies have used the COXPRESdb server to develop a co-expression gene network and construct a hierarchical cluster of differentially expressed genes in monkeypox-infected MK2 cells and damaged osteoarthritis cartilage (58,59). In the present study, several bioinformatics methods and servers (PRECOG, COXPRESdb and STRING) were used to assess gene expression and networks in TMZ-resistant GBM8401 cells. However, one of the limitations of COXPRESdb is that it does not have a feature for searching negative correlations of co-expression, resulting in only positive correlations in the co-expression analysis. In a PPI network, edges symbolize interactions between proteins and nodes symbolize proteins (60). According to the graph theory, the topological structure of a PPI network provides direct and preliminary information related to the network and its biological functions (60,61). The PPI network provides information on different factors, such as genetic cues and signaling circuits. It improves the understanding of circuitry to predict the function of genes and cellular behaviors associated with different signals (62). The present study therefore provides a preliminary understanding of the PPI networks in TMZ-resistant GBM cells; however, to further understand these factors, a broader and more specific study of the PPI network in TMZ-resistant GBM is necessary. Future studies should focus on these topics.

The present study evaluated the upregulated and downregulated genes in wild-type and mutant IDH samples from TMZ-resistant GBM8401 cells. Previous studies have mainly focused on TMZ resistance in IDH wild-type GBM (63-65)

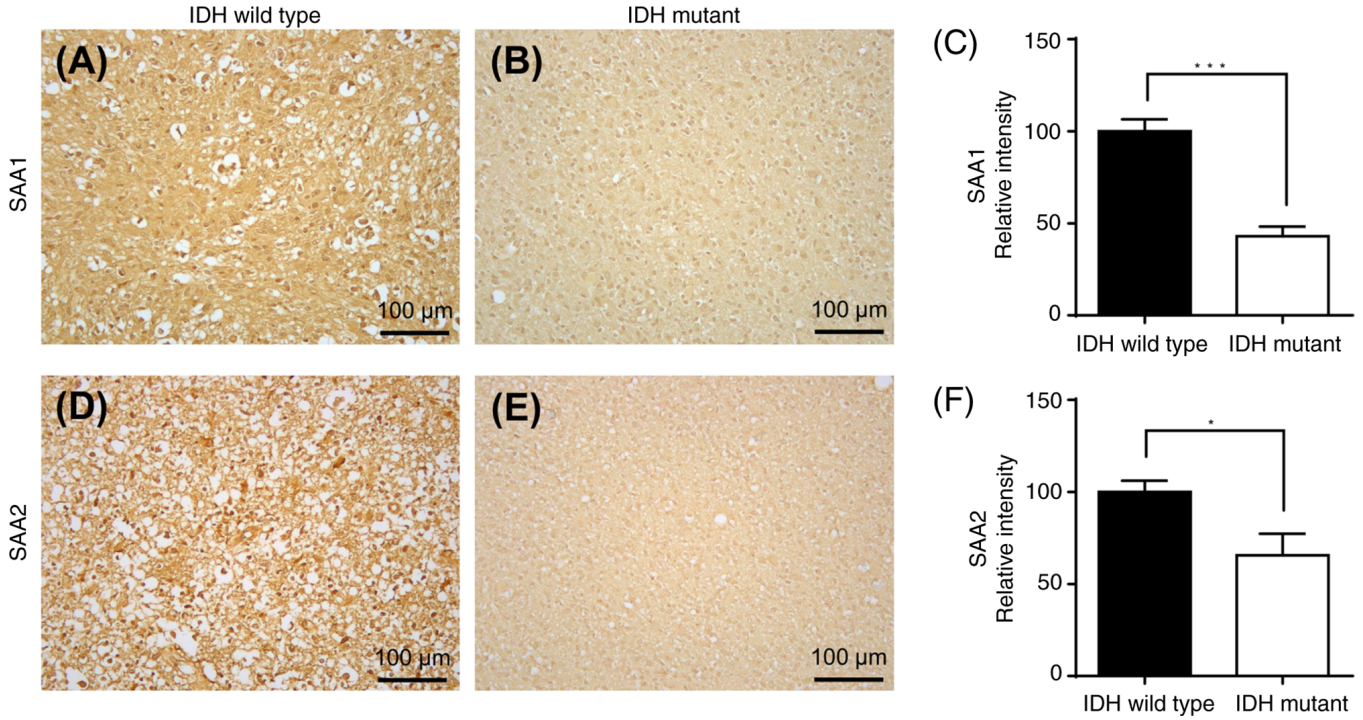


Figure 14. Immunohistochemical staining for SAA1 and SAA2 expression on human GBM samples with either wild-type or mutant IDH. Representative images of SAA1-immunoreactivity in GBM tissues with (A) IDH wild-type and (B) IDH-mutant. (C) SAA1 relative intensity in IDH wild-type and IDH-mutant samples. Representative images of SAA2-immunoreactivity in GBM tissues with (D) IDH wild-type or (E) IDH-mutant. (F) SAA2 relative intensity in IDH wild-type and mutant samples. Values are expressed as the mean ± standard deviation. The data were analyzed using unpaired Student's t-tests. $^{*}$P<0.05; $^{***}$P<0.001. IDH, isocitrate dehydrogenase; SA, serum amyloid; IHC, immunohistochemistry.

and $O^6$-methylguanine-DNA-methyltransferase (66). There is a higher incidence of TMZ-induced hypermutations in IDH-mutant gliomas than in IDH wild-type gliomas (67,68). Exogenously expressed mutant IDH increases TMZ resistance in glioma cells (69). Sun and Turcan (23) also suggested that TMZ treatment may exacerbate IDH mutations in GBM. However, previous studies have not elucidated the possible mechanisms of IDH mutations that contribute to TMZ resistance in GBM, to the best of our knowledge.

*TIE1* is an angiopoietin receptor with immunoglobulin and EGF-like domains 1, and the TIE1 protein is a cell surface protein expressed in endothelial cells (70); however, it is also expressed in immature hematopoietic cells and platelets (71). *TIE1* has an inflammatory effect and may serve a role in mechanotransduction, neovascularization and inflammation. It serves an important role in the development of atherosclerosis (72) and a significant pathophysiological role in the development of several cancers. Therefore, the orphan receptor *TIE1* is a drug target for inhibiting cancer angiogenesis and migration (73). Therefore, it is necessary to understand *TIE1* gene expression patterns in gliomas and GBMs. *CACNA2D1* encodes calcium voltage-gated channel auxiliary subunit α2/Δ1 protein (calcium channel α2δ1 subunit), a membrane protein associated with the voltage-gated calcium channel complex. It serves a role in the influx of calcium ions into calcium channels (74). The CACNA2D1 protein is the molecular target of the gabapentinoid group of molecules, including gabapentin and pregabalin. Gabapentin is a class of anticonvulsant molecules used to treat epilepsy, particularly drug-resistant focal epilepsy (75). Pregabalin is used for the treatment of diabetic neuropathic pain in adults. It is also used to treat neuropathic pain, such as cancer and chemotherapy-induced postherpetic neuralgia, fibromyalgia and diabetic neuropathy (76-78). Understanding *CACNA2D1* gene expression patterns in gliomas, GBMs and other brain tumors is therefore essential. The *CAPN6* gene is encodes the calpain protein. This gene helps in microtubule stabilization and is associated with cytoskeletal organization and regulation of microtubule dynamics (79). The protein belongs to a family of calcium-dependent cysteine proteases that is well conserved in nature (80). CAPN6 may also serve a role in tumor formation by inhibiting apoptosis and promoting angiogenesis (81). Therefore, *CAPN6* gene expression patterns should be studied in GBM and other brain tumors. *ADAMTS6* encodes ADAM metallopeptidase with six thrombospondin type 1 motif proteins, which are members of the ADAMTS protein family (82). Researchers have reported that cytokine TNF-α may regulate the expression of a gene, which may be *ADAMTS6*. Similarly, it has been reported that *ADAMTS6* restrains tumor development through the ERK signaling pathway (83); however, further studies are required to understand the *ADAMTS6* gene in GBM and its resistance.

*SAA1* and *SAA2* are two significant and highly homologous genes (84,85). The *SAA1* gene encodes the SAA1 protein, which is considered to be an 'acute response protein'. This gene is expressed in hepatocytes, amnion fibroblasts, the epithelium of the amnion and trophoblasts of the chorion (86) and is expressed in tissue injury, infection, chronic inflammation and cancers such as renal cancer (87,88). *SAA1* expression patterns should be studied

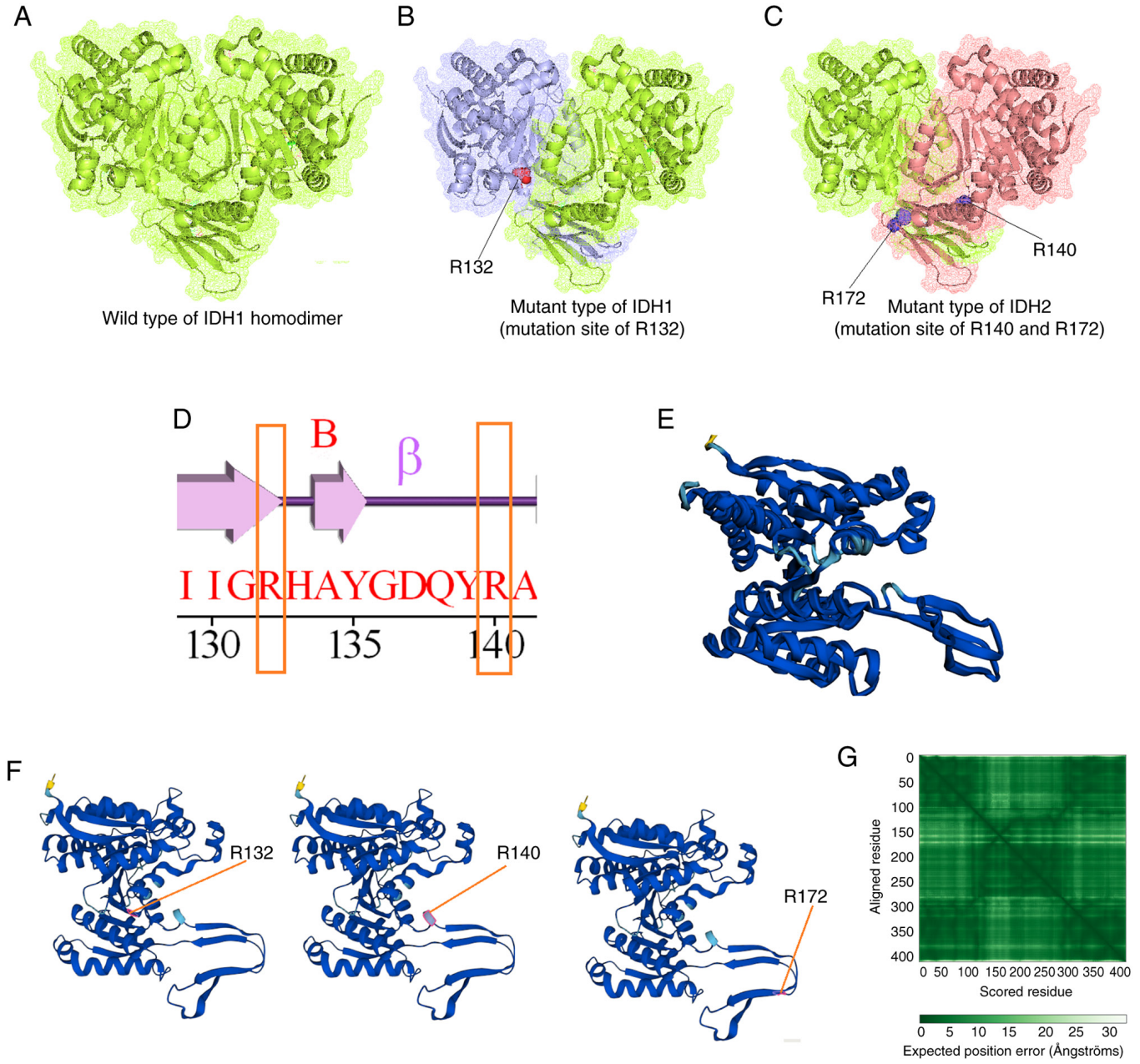


Figure 15. Mutational landscape of IDH in glioblastoma multiforme. (A) Homodimer structure of wild-type IDH1. (B) Mutant-type IDH1and its mutation residue position at R132. (C) Mutant-type IDH2 and its mutation residue position at R140 or R172. (D) Secondary structural landscape of IDH with a mutation residue position at R132 or R140. (E) IDH 3D structural model developed using AlphaFold. (F) Mutant residue positions (R132, R140 and R172) are shown in the 3D model of IDH, which was developed using AlphaFold. (G) Performance of the 3D structural model was validated by the aligned residues. IDH, isocitrate dehydrogenase; 3D, three-dimensional.

in gliomas, GBMs and other brain cancers, as well as in chemotherapy-resistant brain tumors. Similarly, *SAA2* encodes the SAA2 protein, which is highly conserved during mammalian evolution (89). Furthermore, SAA2 may be expressed in lung cancer cells. Kim *et al* (90) quantified the SAA2 protein in lung cancer plasma. However, the role of *SAA2* in GBM and its resistance to chemotherapy remains unknown and should be investigated. *GDF15* was first identified as a macrophage inhibitory cytokine that encodes the GDF15 protein and belongs to the TGF-β superfamily (91). Elevated GDF15 levels have also been observed in patients with autoimmune diseases (91,92). GDF15 has a functional association with Ras suppressor-1 in cancer cell invasion and may act as a drug target for cancers, such as breast cancer (93). The *USP26* gene encodes a member of a family of ubiquitin-specific processing proteins, and it is an X chromosome-linked deubiquitinase. This gene has a distinct role in spermatogenesis (94). Recently, Guo *et al* (95) reported an association between *GDF15* gene expression and malignant progression in gliomas. *USP26* gene expression patterns in gliomas, GBMs and chemotherapy-resistant brain tumors should be investigated.

Furthermore, a relationship between *SAA1* upregulation and TMZ resistance in GBM may exist, and *SAA1* upregulation may promote TMZ resistance. Zhang *et al* (96) reported that *SAA1* knockdown promoted GBM cell apoptosis through

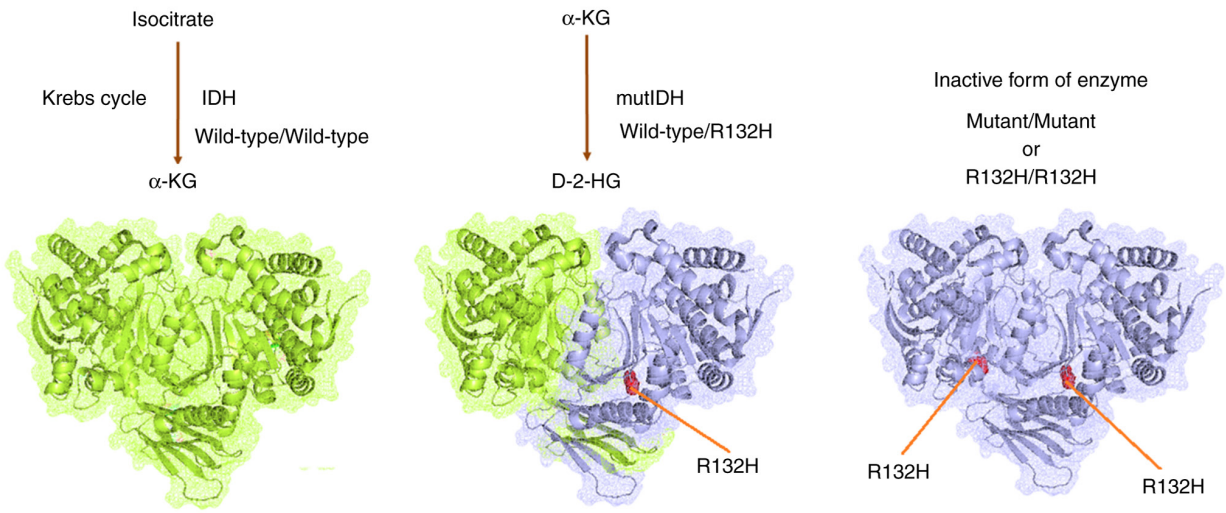


Figure 16. Hypothetical mechanism to illustrate the IDH-mutated glioblastoma multiforme landscape. IDH, isocitrate dehydrogenase; α-KG, α-ketoglutarate; D-2HG, D-(R)-2-hydroxyglutarate; Mut, mutant.

PI3K/Akt signaling. Moreover, Singh *et al* (48) reported the role of the PI3K/Akt signaling pathway in TMZ-resistant GBM. Therefore, *SAA1* may serve a role in TMZ-resistant GBM via the PI3K/Akt signaling pathway. However, further studies are needed to confirm this hypothesis. Similarly, other than the PI3K/Akt signaling pathway, the involvement of the tricarboxylic acid (TCA) cycle has been noted in TMZ-resistant GBM as IDH enzymes are the prime components of the TCA cycle. Therefore, the TCA cycle may be associated with TMZ-resistant GBM (97). However, Immanuel *et al* (98) investigated the metabolic landscapes associated with oxidative phosphorylation pathways, the malate-aspartate shunt, glycolysis and the TCA cycle, which are linked with the oxidative phosphorylation of neuronal cells, and potentially, TMZ-resistant GBM.

Among the genes assessed in the present study, certain genes were found to serve a role in cell differentiation and the relative tumor response. For example, *SAA1* and *SAA2* serve potential roles in cell differentiation. Lee *et al* (99) reported that SA proteins (SAA1 and SAA2) promote Th17 cell differentiation. Additionally, Takehara *et al* (100) reported that *SAA1* expression promotes cancer cell progression. *SAA1* may also serve a role in cancer cell differentiation and progression. Similarly, studies have shown that GDF15, a mitochondrial cytokine (mitokine), induces cancer cell subpopulations and provides an invasive advantage. Kang *et al* (101) reported that GDF15 expression in tumors is associated with tumor aggressiveness and that GDF15 influences STAT3 activation, which assists in thyroid cancer tumor progression. They also reported that GDF15 acts via the STAT3 signaling axis. Similarly, Wosnitzer *et al* (102) reported that the expression of the *USP26* gene promotes cell differentiation and induces tumorigenesis.

IDH mutations are among the most critical and earliest genomic alterations in GBM progression and recurrence (24). IDH enzymes catalyze the conversion of isocitrate to α-KG, an intermediate in the citric acid cycle that contributes to NADPH production (103). The IDH mutation produces neomorphic enzymatic activity that converts α-KG to D-2-HG, leading to the accumulation of 2-HG and inhibition of α-KG-dependent enzymes such as histone and DNA demethylases in the tumor (104). The role of IDH mutations has also been explored in other brain tumors (105). Therefore, it is necessary to understand the role of IDH mutations in GBM progression. The present study assessed the mutational landscape of IDH in GBM through *in silico* models. Therefore, the findings of the present study are important for understanding the role of IDH mutations in GBM progression. However, future research is required to enhance the understanding of the complete molecular mechanisms underlying IDH mutations in GBM progression.

The present study identified the gene expression profiles of TMZ-resistant GBM, mainly the upregulated and downregulated genes and the IDH mutational landscapes in GBM. The mapped genes will help future researchers understand the association between these upregulated and downregulated genes and the development of TMZ resistance. Specifically, previous studies reported that there may be an indirect relationship between the *SAA1* gene and TMZ-resistant GBM through the PI3K/Akt signaling pathway (48,96); however, future studies are needed to assess the hypothesis. Additionally, a previous study reported that *GDF15* promotes the upregulation of the programmed death-ligand 1 (PD-L1) protein expression in glioblastoma (106); however, no direct evidence indicates that the upregulation of *GDF15* promotes TMZ resistance. Nevertheless, a study reported that TMZ-mediated PD-L1 expression in GBM cells and knockdown of *PD-L1* impaired the TMZ-induced inhibition effect of GBM cells (107). Therefore, we hypothesize that *GDF15* is likely to be involved in TMZ resistance through the regulation of *PD-L1*. Furthermore, CACNA2D3 is a tumor suppressor in gliomas (108) and can enhance the chemosensitivity of esophageal squamous cell carcinoma (109). It is also one of the objectives worthy of future exploration.

In the future, the targeted genes whose expression levels increase (*SAA1*, *SAA2*, *GDF15* and *USP26*) or decrease (*TIE1*, *CACNA2D1*, *CAPN*, and *ADAMTS6*) in TMZ-resistance GBM will be manipulated by gene knockdown (e.g., using

siRNA) or gene overexpression (e.g., via transfection plasmid), respectively. Further research should investigate whether the cytotoxic sensitivity to TMZ of TMZ-resistant GBM cells can be altered and the molecular mechanisms involved, in order to understand TMZ resistance in GBM from a molecular mechanistic viewpoint, which may help solve the MDR problem.

However, researchers are attempting to fight GBM from different directions, and therefore, rapid progress has been made in GBM research to combat tumors. For example, the 3D bioprinting of neural cells is essential for understanding neural cells and their therapeutics (110). Dai *et al* (111) developed a 3D-bioprinted model in which glioblastoma stem cells (GSCs) and mesenchymal stem cells (MSCs) were fused. This will aid in understanding the interaction between GSCs and MSCs and explain tumor progression. Interactions between NSCs and microglial cells have also been studied through single-cell whole-transcriptome sequencing, which helps to further understand the recurrence of GBM (112). Additionally, Liu *et al* (113) developed ultra-small zirconium carbide nanoparticles to treat gliomas.

The present study has some limitations. Firstly, during immunohistochemical staining, the expression of *TIE1* and *CAPN6* genes, and *SAA1* and *SAA2* genes was studied. The expression of other genes was not studied through immunohistochemical staining due to the lack of availability of other antibodies. Secondly, the study depended on the servers' dataset for bioinformatics analysis. For example, the PRECOG server dataset was used during the KM survival and meta-Z analyses. However, these servers are highly cited.

In conclusion, GBM is a complex heterogeneous disease and chemoresistance is a significant issue in patients with GBM. To this end, the present comprehensive study identified the downregulated and upregulated genes and their expression patterns. This simplifies the current understanding of this complex disease and TMZ resistance. NGS and RNA-seq analyses identified upregulated and downregulated genes in the GBM8401-resistant cells. The present study also illustrated the mutational landscape of IDH in GBM, which suggested that the IDH mutational landscape contributes to TMZ resistance in GBM cells. The results of the present study provide possible mechanisms for IDH mutations that contribute to TMZ resistance in GBM. They also provide significant insights into the molecular mechanisms of resistance in GBM. The present study also provides directions that may assist in future therapeutic developments related to IDH mutations. A deeper understanding of TMZ resistance in GBM may help solve the MDR problem. Therefore, the results of the present study are important for future researchers to develop novel biomarkers and therapeutics for brain tumors. These findings will help to identify the underlying molecular mechanisms and signaling networks, appropriate biomarkers, new therapeutic targets and novel therapeutics for GBM and other brain tumors.

## Acknowledgements

The authors would like to thank Chang Gung Medical Foundation Kaohsiung Chang Gung Memorial Hospital Biobank & Research Specimen Processing Lab for patient sample preparation and sectioning.

## Funding

The present study was supported by research grants from the National Science and Technology Council (grant nos. 109-2314-B-182A-080-MY2 and 111-2314-B-182A-132-MY3) and Chang Gung Memorial Hospital (grant nos. CMRPG8K1403 and CMRPG8N1461).

## Availability of data and materials

The RNA-seq data generated in the present study may be found in the NCBI Gene Expression Omnibus under the GEO Series accession number GSE234762 or at the following URL (https://www.ncbi.nlm.nih.gov/geo/query/acc.cgi?acc=GSE234762). All other data generated in the present study may be requested from the corresponding author.

## Authors' contributions

WFC, ZHW and CC wrote the manuscript, performed analyses and sketched the figures and tables. JMJC, NFC, SNY and MB performed formal analyses and validation. HTL and KD performed the analysis and/or interpretation of data, and the review of the manuscript. WFC and ZHW confirm the authenticity of all the raw data. All authors have read and approved the final manuscript.

## Ethics approval and consent to participate

The present study was approved by the Chang Gung Medical Foundation Institutional Review Board (approval no. 201902218B1B0). Written informed consent was obtained before collecting the samples.

## Patient consent for publication

Not applicable.

## Competing interests

The authors declare that they have no competing interests.

## References

1. Grech N, Dalli T, Mizzi S, Meilak L, Calleja N and Zrinzo A: Rising incidence of glioblastoma multiforme in a well-defined population. Cureus 12: e8195, 2020.
2. Miller KD, Ostrom QT, Kruchko C, Patil N, Tihan T, Cioffi G, Fuchs HE, Waite KA, Jemal A, Siegel RL and Barnholtz-Sloan JS: Brain and other central nervous system tumor statistics, 2021. CA Cancer J Clin 71: 381-406, 2021.
3. Ostrom QT, Cioffi G, Waite K, Kruchko C and Barnholtz-Sloan JS: CBTRUS statistical report: Primary brain and other central nervous system tumors diagnosed in the United States in 2014-2018. Neuro Oncol 23 (12 Suppl 2): iii1-iii105, 2021.
4. Wen PY and Kesari S: Malignant gliomas in adults. N Engl J Med 359: 492-507, 2008.
5. Kleihues P and Ohgaki H: Primary and secondary glioblastomas: From concept to clinical diagnosis. Neuro Oncol 1: 44-51, 1999.
6. Lin D, Wang M, Chen Y, Gong J, Chen L, Shi X, Lan F, Chen Z, Xiong T, Sun H and Wan S: Trends in Intracranial glioma incidence and mortality in the United States, 1975-2018. Front Oncol 11: 748061, 2021.
7. Upadhyaya SA, Ghazwani Y, Wu S, Broniscer A, Boop FA, Gajjar A and Qaddoumi I: Mortality in children with low-grade glioma or glioneuronal tumors: A single-institution study. Pediatr Blood Cancer 65: 10.1002/pbc.26717, 2018.

8. Yao M, Li S, Wu X, Diao S, Zhang G, He H, Bian L and Lu Y: Cellular origin of glioblastoma and its implication in precision therapy. Cell Mol Immunol 15: 737-739, 2018.
9. Louis DN, Perry A, Reifenberger G, von Deimling A, Figarella-Branger D, Cavenee WK, Ohgaki H, Wiestler OD, Kleihues P and Ellison DW: The 2016 World Health Organization classification of tumors of the central nervous system: A summary. Acta Neuropathol 131: 803-820, 2016.
10. Stupp R, Mason WP, van den Bent MJ, Weller M, Fisher B, Taphoorn MJ, Belanger K, Brandes AA, Marosi C, Bogdahn U, *et al*: Radiotherapy plus concomitant and adjuvant temozolomide for glioblastoma. N Engl J Med 352: 987-996, 2005.
11. Olivier C, Oliver L, Lalier L and Vallette FM: Drug resistance in glioblastoma: The two faces of oxidative stress. Front Mol Biosci 7: 620677, 2021.
12. Mansoori B, Mohammadi A, Davudian S, Shirjang S and Baradaran B: The different mechanisms of cancer drug resistance: A brief review. Adv Pharm Bull 7: 339-348, 2017.
13. Jakoby WB: The glutathione S-transferases: A group of multifunctional detoxification proteins. Adv Enzymol Relat Areas Mol Biol 46: 383-414, 1978.
14. Oliver L, Lalier L, Salaud C, Heymann D, Cartron PF and Vallette FM: Drug resistance in glioblastoma: Are persisters the key to therapy? Cancer Drug Resist 3: 287-301, 2020.
15. Phi LTH, Sari IN, Yang YG, Lee SH, Jun N, Kim KS, Lee YK and Kwon HY: Cancer stem cells (CSCs) in drug resistance and their therapeutic implications in cancer treatment. Stem Cells Int 2018: 5416923, 2018.
16. Liu G, Yuan X, Zeng Z, Tunici P, Ng H, Abdulkadir IR, Lu L, Irvin D, Black KL and Yu JS: Analysis of gene expression and chemoresistance of CD133+ cancer stem cells in glioblastoma. Mol Cancer 5: 67, 2006.
17. Behnan J, Finocchiaro G and Hanna G: The landscape of the mesenchymal signature in brain tumours. Brain 142: 847-866, 2019.
18. Yu Z, Chen Y, Wang S, Li P, Zhou G and Yuan Y: Inhibition of NF-κB results in anti-glioma activity and reduces temozolomide-induced chemoresistance by down-regulating MGMT gene expression. Cancer Lett 428: 77-89, 2018.
19. Yao L, Li J, Zhang X, Zhou L and Hu K: Downregulated ferroptosis-related gene SQLE facilitates temozolomide chemoresistance, and invasion and affects immune regulation in glioblastoma. CNS Neurosci Ther 28: 2104-2115, 2022.
20. Cohen AL, Holmen SL and Colman H: IDH1 and IDH2 mutations in gliomas. Curr Neurol Neurosci Rep 13: 345, 2013.
21. Hegi ME, Diserens AC, Gorlia T, Hamou MF, de Tribolet N, Weller M, Kros JM, Hainfellner JA, Mason W, Mariani L, *et al*: MGMT gene silencing and benefit from temozolomide in glioblastoma. N Engl J Med 352: 997-1003, 2005.
22. Perez A and Huse JT: The evolving classification of diffuse gliomas: World Health Organization updates for 2021. Curr Neurol Neurosci Rep 21: 67, 2021.
23. Sun X and Turcan S: From laboratory studies to clinical trials: Temozolomide use in IDH-mutant gliomas. Cells 10: 1225, 2021.
24. Han S, Liu Y, Cai SJ, Qian M, Ding J, Larion M, Gilbert MR and Yang C: IDH mutation in glioma: Molecular mechanisms and potential therapeutic targets. Br J Cancer 122: 1580-1589, 2020.
25. Nobusawa S, Watanabe T, Kleihues P and Ohgaki H: IDH1 mutations as molecular signature and predictive factor of secondary glioblastomas. Clin Cancer Res 15: 6002-6007, 2009.
26. Govindarajan V, Shah AH, Di L, Rivas S, Suter RK, Eichberg DG, Luther E, Lu V, Morell AA, Ivan ME, *et al*: Systematic review of epigenetic therapies for treatment of IDH-mutant glioma. World Neurosurg 162: 47-56, 2022.
27. Qi S, Lei Y, Si G, YanQing D, HuiXia H, XueLin Z, LanXiao W and Fei Y: IDH mutations predict longer survival and response to temozolomide in secondary glioblastoma. Cancer Sci 103: 269-273, 2012.
28. Munoz JL, Bliss SA, Greco SJ, Ramkissoon SH, Ligon KL and Rameshwar P: Delivery of functional anti-miR-9 by mesenchymal stem cell-derived exosomes to glioblastoma multiforme cells conferred chemosensitivity. Mol Ther Nucleic Acids 2: e126, 2013.
29. Bolger AM, Lohse M and Usadel B: Trimmomatic: A flexible trimmer for Illumina sequence data. Bioinformatics 30: 2114-2120, 2014.
30. Pertea M, Kim D, Pertea GM, Leek JT and Salzberg SL: Transcript-level expression analysis of RNA-seq experiments with HISAT, StringTie and Ballgown. Nat Protoc 11: 1650-1667, 2016.
31. Trapnell C, Roberts A, Goff L, Pertea G, Kim D, Kelley DR, Pimentel H, Salzberg SL, Rinn JL and Pachter L: Differential gene and transcript expression analysis of RNA-seq experiments with TopHat and Cufflinks. Nat Protoc 7: 562-578, 2012.
32. Livak KJ and Schmittgen TD: Analysis of relative gene expression data using real-time quantitative PCR and the 2(-Delta Delta C(T)) method. Methods 25: 402-408, 2001.
33. Gentles AJ, Newman AM, Liu CL, Bratman SV, Feng W, Kim D, Nair VS, Xu Y, Khuong A, Hoang CD, *et al*: The prognostic landscape of genes and infiltrating immune cells across human cancers. Nat Med 21: 938-945, 2015.
34. Dudley WN, Wickham R and Coombs N: An introduction to survival statistics: Kaplan-Meier analysis. J Adv Pract Oncol 7: 91-100, 2016.
35. Lubbock ALR, Katz E, Harrison DJ and Overton IM: TMA navigator: Network inference, patient stratification and survival analysis with tissue microarray data. Nucleic Acids Res 41 (Web Server Issue): W562-W568, 2013.
36. Stelzer G, Dalah I, Stein TI, Satanower Y, Rosen N, Nativ N, Oz-Levi D, Olender T, Belinky F, Bahir I, *et al*: In-silico human genomics with GeneCards. Hum Genomics 5: 709-717, 2011.
37. Stelzer G, Rosen N, Plaschkes I, Zimmerman S, Twik M, Fishilevich S, Stein TI, Nudel R, Lieder I, Mazor Y, *et al*: The GeneCards suite: From gene data mining to disease genome sequence analyses. Curr Protoc Bioinformatics 54: 1.30.1-1.30.33, 2016.
38. Szklarczyk D, Franceschini A, Wyder S, Forslund K, Heller D, Huerta-Cepas J, Simonovic M, Roth A, Santos A, Tsafou KP, *et al*: STRING v10: Protein-protein interaction networks, integrated over the tree of life. Nucleic Acids Res 43 (Database Issue): D447-D452, 2015.
39. Maglott D, Ostell J, Pruitt KD and Tatusova T: Entrez gene: Gene-centered information at NCBI. Nucleic Acids Res 33 (Database Issue): D54-D58, 2005.
40. Crowe AR and Yue W: Semi-quantitative determination of protein expression using immunohistochemistry staining and analysis: An Integrated Protocol. Bio Protoc 9: e3465, 2019.
41. Yuan JX and Munson JM: Quantitative immunohistochemistry of the cellular microenvironment in patient glioblastoma resections. J Vis Exp: 56025, 2017.
42. Burley SK, Berman HM, Kleywegt GJ, Markley JL, Nakamura H and Velankar S: Protein data bank (PDB): The single global macromolecular structure archive. Methods Mol Biol 1607: 627-641, 2017.
43. Yuan S, Chan HCS, Filipek S and Vogel H: PyMOL and inkscape bridge the data and the data visualization. Structure 24: 2041-2042, 2016.
44. Jumper J, Evans R, Pritzel A, Green T, Figurnov M, Ronneberger O, Tunyasuvunakool K, Bates R, Žídek A, Potapenko A, *et al*: Highly accurate protein structure prediction with AlphaFold. Nature 596: 583-589, 2021.
45. de Beer TAP, Berka K, Thornton JM and Laskowski RA: PDBsum additions. Nucleic Acids Res 42 (Database Issue): D292-D296, 2014.
46. Hammer Ø, Harper DAT and Ryan PD: PAST: Paleontological statistics software package for education and data analysis. Palaeontol Electron 4: 9, 2001.
47. MATLAB: High performance numeric computation and visualization software: User's guide: For UNIX workstations. Mathworks Incorporated, 2003.
48. Singh N, Miner A, Hennis L and Mittal S: Mechanisms of temozolomide resistance in glioblastoma-a comprehensive review. Cancer Drug Resist 4: 17-43, 2021.
49. Chen X, Zhang M, Gan H, Wang H, Lee JH, Fang D, Kitange GJ, He L, Hu Z, Parney IF, *et al*: A novel enhancer regulates MGMT expression and promotes temozolomide resistance in glioblastoma. Nat Commun 9: 2949, 2018.
50. Bukowski K, Kciuk M and Kontek R: Mechanisms of multidrug resistance in cancer chemotherapy. Int J Mol Sci 21: 3233, 2020.
51. Rapin N, Bagger FO, Jendholm J, Mora-Jensen H, Krogh A, Kohlmann A, Thiede C, Borregaard N, Bullinger L, Winther O, *et al*: Comparing cancer vs normal gene expression profiles identifies new disease entities and common transcriptional programs in AML patients. Blood 123: 894-904, 2014.
52. Cheng SY, Chen NF, Wen ZH, Yao ZK, Tsui KH, Kuo HM and Chen WF: Glutathione S-transferase M3 is associated with glycolysis in intrinsic temozolomide-resistant glioblastoma multiforme cells. Int J Mol Sci 22: 7080, 2021.
53. Gordinier ME, Schau GF, Pollock SB, Shields LBE and Talwalkar S: Genomic characterization of vulvar squamous cell carcinoma reveals differential gene expression based on clinical outcome. Gynecol Oncol 180: 111-117, 2024.
54. Hu G, Wei B, Wang L, Wang L, Kong D, Jin Y and Sun Z: Analysis of gene expression profiles associated with glioma progression. Mol Med Rep 12: 1884-1890, 2015.

55. Kothari C, Osseni MA, Agbo L, Ouellette G, Déraspe M, Laviolette F, Corbeil J, Lambert JP, Diorio C and Durocher F: Machine learning analysis identifies genes differentiating triple negative breast cancers. Sci Rep 10: 10464, 2020.
56. Kumar SU, Kumar DT, Siva R, Doss CGP and Zayed H: Integrative bioinformatics approaches to map potential novel genes and pathways involved in ovarian cancer. Front Bioeng Biotechnol 7: 391, 2019.
57. Chakraborty C, Sharma AR, Bhattacharya M, Zayed H and Lee SS: Understanding gene expression and transcriptome profiling of COVID-19: An initiative towards the mapping of protective immunity genes against SARS-CoV-2 infection. Front Immunol 12: 724936, 2021.
58. Chakraborty C, Bhattacharya M, Dhama K and Lee SS: Evaluation of differentially expressed genes during replication using gene expression landscape of monkeypox-infected MK2 cells: A bioinformatics and systems biology approach to understanding the genomic pattern of viral replication. J Infect Public Health 16: 399-409, 2023.
59. Dunn SL, Soul J, Anand S, Schwartz JM, Boot-Handford RP and Hardingham TE: Gene expression changes in damaged osteoarthritic cartilage identify a signature of non-chondrogenic and mechanical responses. Osteoarthritis Cartilage 24: 1431-1440, 2016.
60. Chen SJ, Liao DL, Chen CH, Wang TY and Chen KC: Construction and analysis of protein-protein interaction network of heroin use disorder. Sci Rep 9: 4980, 2019.
61. Raman K: Construction and analysis of protein-protein interaction networks. Autom Exp 2: 2, 2010.
62. Silverbush D and Sharan R: A systematic approach to orient the human protein-protein interaction network. Nat Commun 10: 3015, 2019.
63. Lee SY: Temozolomide resistance in glioblastoma multiforme. Genes Dis 3: 198-210, 2016.
64. Mrugala MM and Chamberlain MC: Mechanisms of disease: Temozolomide and glioblastoma-look to the future. Nat Clin Pract Oncol 5: 476-486, 2008.
65. Woo PYM, Li Y, Chan AHY, Ng SCP, Loong HHF, Chan DTM, Wong GKC and Poon WS: A multifaceted review of temozolomide resistance mechanisms in glioblastoma beyond O-6-methylguanine-DNA methyltransferase. Glioma 2: 68-82, 2019.
66. Kitange GJ, Carlson BL, Schroeder MA, Grogan PT, Lamont JD, Decker PA, Wu W, James CD and Sarkaria JN: Induction of MGMT expression is associated with temozolomide resistance in glioblastoma xenografts. Neuro Oncol 11: 281-291, 2009.
67. Barthel FP, Johnson KC, Varn FS, Moskalik AD, Tanner G, Kocakavuk E, Anderson KJ, Abiola O, Aldape K, Alfaro KD, *et al*: Longitudinal molecular trajectories of diffuse glioma in adults. Nature 576: 112-120, 2019.
68. Jonsson P, Lin AL, Young RJ, DiStefano NM, Hyman DM, Li BT, Berger MF, Zehir A, Ladanyi M, Solit DB, *et al*: Genomic correlates of disease progression and treatment response in prospectively characterized gliomas. Clin Cancer Res 25: 5537-5547, 2019.
69. Ohba S, Mukherjee J, See WL and Pieper RO: Mutant IDH1-driven cellular transformation increases RAD51-mediated homologous recombination and temozolomide resistance. Cancer Res 74: 4836-4844, 2014.
70. Chen T, Wang J, Xue B, Kong Q, Liu Z and Yu B: Identification and characterization of a novel porcine endothelial cell-specific Tie1 promoter. Xenotransplantation 20: 438-448, 2013.
71. Rodewald HR and Sato TN: Tie1, a receptor tyrosine kinase essential for vascular endothelial cell integrity, is not critical for the development of hematopoietic cells. Oncogene 12: 397-404, 1996.
72. Woo KV and Baldwin HS: Role of Tie1 in shear stress and atherosclerosis. Trends Cardiovasc Med 21: 118-123, 2011.
73. Meltzer M, Eliash N, Azoulay Z, Hadad U and Papo N: In vitro inhibition of cancer angiogenesis and migration by a nanobody that targets the orphan receptor Tie1. Cell Mol Life Sci 79: 312, 2022.
74. Dolphin AC: Voltage-gated calcium channel $\alpha_2\delta$ subunits: an assessment of proposed novel roles. F1000Res 7: F1000 Faculty Rev-1830, 2018.
75. Panebianco M, Al-Bachari S, Hutton JL and Marson AG: Gabapentin add-on treatment for drug-resistant focal epilepsy. Cochrane Database Syst Rev 1: CD001415, 2021.
76. Derry S, Bell RF, Straube S, Wiffen PJ, Aldington D and Moore RA: Pregabalin for neuropathic pain in adults. Cochrane Database Syst Rev 1: CD007076, 2019.
77. Alles SRA, Cain SM and Snutch TP: Pregabalin as a pain therapeutic: Beyond calcium channels. Front Cell Neurosci 14: 83, 2020.
78. Verma V, Singh N and Singh Jaggi A: Pregabalin in neuropathic pain: Evidences and possible mechanisms. Curr Neuropharmacol 12: 44-56, 2014.
79. Tonami K, Kurihara Y, Aburatani H, Uchijima Y, Asano T and Kurihara H: Calpain 6 is involved in microtubule stabilization and cytoskeletal organization. Mol Cell Biol 27: 2548-2561, 2007.
80. Ono Y and Sorimachi H: Calpains: An elaborate proteolytic system. Biochim Biophys Acta 1824: 224-236, 2012.
81. Chen L, Xiao D, Tang F, Gao H and Li X: CAPN6 in disease: An emerging therapeutic target (review). Int J Mol Med 46: 1644-1652, 2020.
82. Kelwick R, Desanlis I, Wheeler GN and Edwards DR: The ADAMTS (a disintegrin and metalloproteinase with thrombospondin motifs) family. Genome Biol 16: 113, 2015.
83. Xie Y, Gou Q, Xie K, Wang Z, Wang Y and Zheng H: ADAMTS6 suppresses tumor progression via the ERK signaling pathway and serves as a prognostic marker in human breast cancer. Oncotarget 7: 61273-61283, 2016.
84. Mori M, Tian G, Ishikawa A and Higuchi K: Diversity and complexity of the mouse Saa1 and Saa2 genes. Exp Anim 63: 99-106, 2014.
85. Jumeau C, Awad F, Assrawi E, Cobret L, Duquesnoy P, Giurgea I, Valeyre D, Grateau G, Amselem S, Bernaudin JF and Karabina SA: Expression of SAA1, SAA2 and SAA4 genes in human primary monocytes and monocyte-derived macrophages. PLoS One 14: e0217005, 2019.
86. Li W, Wang W, Zuo R, Liu C, Shu Q, Ying H and Sun K: Induction of pro-inflammatory genes by serum amyloid A1 in human amnion fibroblasts. Sci Rep 7: 693, 2017.
87. Abouelasrar Salama S, De Bondt M, De Buck M, Berghmans N, Proost P, Oliveira VLS, Amaral FA, Gouwy M, Van Damme J and Struyf S: Serum amyloid A1 (SAA1) revisited: Restricted leukocyte-activating properties of homogeneous SAA1. Front Immunol 11: 843, 2020.
88. Li S, Cheng Y, Cheng G, Xu T, Ye Y, Miu Q, Cao Q, Yang X, Ruan H and Zhang X: High SAA1 expression predicts advanced tumors in renal cancer. Front Oncol 11: 649761, 2021.
89. Sack GH Jr: Serum amyloid A-a review. Mol Med 24: 46, 2018.
90. Kim YJ, Gallien S, El-Khoury V, Goswami P, Sertamo K, Schlesser M, Berchem G and Domon B: Quantification of SAA1 and SAA2 in lung cancer plasma using the isotype-specific PRM assays. Proteomics 15: 3116-3125, 2015.
91. Wischhusen J, Melero I and Fridman WH: Growth/differentiation factor-15 (GDF-15): From biomarker to novel targetable immune checkpoint. Front Immunol 11: 951, 2020.
92. Arinaga-Hino T, Ide T, Akiba J, Suzuki H, Kuwahara R, Amano K, Kawaguchi T, Sano T, Inoue E, Koga H, *et al*: Growth differentiation factor 15 as a novel diagnostic and therapeutic marker for autoimmune hepatitis. Sci Rep 12: 8759, 2022.
93. Gkretsi V, Louca M, Stylianou A, Minadakis G, Spyrou GM and Stylianopoulos T: Inhibition of breast cancer cell invasion by ras suppressor-1 (RSU-1) silencing is reversed by growth differentiation factor-15 (GDF-15). Int J Mol Sci 20: 163, 2019.
94. Sakai K, Ito C, Wakabayashi M, Kanzaki S, Ito T, Takada S, Toshimori K, Sekita Y and Kimura T: Usp26 mutation in mice leads to defective spermatogenesis depending on genetic background. Sci Rep 9: 13757, 2019.
95. Guo L, Chen Y, Hu S, Gao L, Tang N, Liu R, Qin Y, Ren C and Du S: GDF15 expression in glioma is associated with malignant progression, immune microenvironment, and serves as a prognostic factor. CNS Neurosci Ther 28: 158-171, 2022.
96. Zhang H, Xu Y, Deng G, Yuan F, Tan Y, Gao L, Sun Q, Qi Y, Yang K, Geng R and Jiang H: SAA1 knockdown promotes the apoptosis of glioblastoma cells via downregulation of AKT signaling. J Cancer 12: 2756-2767, 2021.
97. Tommasini-Ghelfi S, Murnan K, Kouri FM, Mahajan AS, May JL and Stegh AH: Cancer-associated mutation and beyond: The emerging biology of isocitrate dehydrogenases in human disease. Sci Adv 5: eaaw4543, 2019.
98. Immanuel SRC, Ghanate AD, Parmar DS, Yadav R, Uthup R, Panchagnula V and Raghunathan A: Integrated genetic and metabolic landscapes predict vulnerabilities of temozolomide resistant glioblastoma cells. NPJ Syst Biol Appl 7: 2, 2021.
99. Lee JY, Hall JA, Kroehling L, Wu L, Najar T, Nguyen HH, Lin WY, Yeung ST, Silva HM, Li D, *et al*: Serum amyloid A proteins induce pathogenic Th17 cells and promote inflammatory disease. Cell 180: 79-91.e16, 2020.

100. Takehara M, Sato Y, Kimura T, Noda K, Miyamoto H, Fujino Y, Miyoshi J, Nakamura F, Wada H, Bando Y, *et al*: Cancer-associated adipocytes promote pancreatic cancer progression through SAA1 expression. Cancer Sci 111: 2883-2894, 2020.
101. Kang YE, Kim JM, Lim MA, Lee SE, Yi S, Kim JT, Oh C, Liu L, Jin Y, Jung SN, *et al*: Growth differentiation factor 15 is a cancer cell-induced mitokine that primes thyroid cancer cells for invasiveness. Thyroid 31: 772-786, 2021.
102. Wosnitzer MS, Mielnik A, Dabaja A, Robinson B, Schlegel PN and Paduch DA: Ubiquitin specific protease 26 (USP26) expression analysis in human testicular and extragonadal tissues indicates diverse action of USP26 in cell differentiation and tumorigenesis. PLoS One 9: e98638, 2014.
103. Parker SJ and Metallo CM: Metabolic consequences of oncogenic IDH mutations. Pharmacol Ther 152: 54-62, 2015.
104. Dang L, White DW, Gross S, Bennett BD, Bittinger MA, Driggers EM, Fantin VR, Jang HG, Jin S, Keenan MC, *et al*: Cancer-associated IDH1 mutations produce 2-hydroxyglutarate. Nature 462: 739-744, 2009.
105. Turkalp Z, Karamchandani J and Das S: IDH mutation in glioma: New insights and promises for the future. JAMA Neurol 71: 1319-1325, 2014.
106. Peng H, Li Z, Fu J and Zhou R: Growth and differentiation factor 15 regulates PD-L1 expression in glioblastoma. Cancer Manag Res 11: 2653-2661, 2019.
107. Wang S, Yao F, Lu X, Li Q, Su Z, Lee JH, Wang C and Du L: Temozolomide promotes immune escape of GBM cells via upregulating PD-L1. Am J Cancer Res 9: 1161-1171, 2019.
108. Jin Y, Cui D, Ren J, Wang K, Zeng T and Gao L: CACNA2D3 is downregulated in gliomas and functions as a tumor suppressor. Mol Carcinog 56: 945-959, 2017.
109. Nie C, Qin X, Li X, Tian B, Zhao Y, Jin Y, Li Y, Wang Q, Zeng D, Hong A and Chen X: CACNA2D3 enhances the chemosensitivity of esophageal squamous cell carcinoma to cisplatin via inducing $Ca^{2+}$-mediated apoptosis and suppressing PI3K/Akt pathways. Front Oncol 9: 185, 2019.
110. Dai X, Tian X, Gu S, Yang Y, Li H, Gao P, Lan Q and Cheng H: Hybrid biofabrication of neurosecretory structures as a model for neurosecretion. Int J Bioprint 9: 659, 2022.
111. Dai X, Shao Y, Tian X, Cao X, Ye L, Gao P, Cheng H and Wang X: Fusion between glioma stem cells and mesenchymal stem cells promotes malignant progression in 3D-bioprinted models. ACS Appl Mater Interfaces 14: 35344-35356, 2022.
112. Dai X, Ye L, Li H, Dong X, Tian H, Gao P, Dong J and Cheng H: Crosstalk between microglia and neural stem cells influences the relapse of glioblastoma in GBM immunological microenvironment. Clin Immunol 251: 109333, 2023.
113. Liu D, Dai X, Zhang W, Zhu X, Zha Z, Qian H, Cheng L and Wang X: Liquid exfoliation of ultrasmall zirconium carbide nanodots as a noninflammatory photothermal agent in the treatment of glioma. Biomaterials 292: 121917, 2023.